

The Vesicle-Forming 6K₂ Protein of Turnip Mosaic Virus Interacts with the COPII Coatomer Sec24a for Viral Systemic Infection

Jun Jiang,^a Camilo Patarroyo,^b Daniel Garcia Cabanillas,^a Huanquan Zheng,^b Jean-François Laliberté^a

INRS-Institut Armand-Frappier, Laval, Québec, Canada^a; Department of Biology, McGill University, Montréal, Québec, Canada^b

ABSTRACT

Positive-sense RNA viruses remodel host cell endomembranes to generate quasi-organelles known as “viral factories” to coordinate diverse viral processes, such as genome translation and replication. It is also becoming clear that enclosing viral RNA (vRNA) complexes within membranous structures is important for virus cell-to-cell spread throughout the host. In plant cells infected by turnip mosaic virus (TuMV), a member of the family *Potyviridae*, peripheral motile endoplasmic reticulum (ER)-derived viral vesicles are produced that carry the vRNA to plasmodesmata for delivery into adjacent noninfected cells. The viral protein 6K₂ is responsible for the formation of these vesicles, but how 6K₂ is involved in their biogenesis is unknown. We show here that 6K₂ is associated with cellular membranes. Deletion mapping and site-directed mutagenesis experiments defined a soluble N-terminal 12-amino-acid stretch, in particular a potyviral highly conserved tryptophan residue and two lysine residues that were important for vesicle formation. When the tryptophan residue was changed into an alanine in the viral polyprotein, virus replication still took place, albeit at a reduced level, but cell-to-cell movement of the virus was abolished. Yeast (*Saccharomyces cerevisiae*) two-hybrid and coimmunoprecipitation experiments showed that 6K₂ interacted with Sec24a, a COPII coatomer component. Appropriately, TuMV systemic movement was delayed in an *Arabidopsis thaliana* mutant line defective in Sec24a. Intercellular movement of TuMV replication vesicles thus requires ER export of 6K₂, which is mediated by the interaction of the N-terminal domain of the viral protein with Sec24a.

IMPORTANCE

Many plant viruses remodel the endoplasmic reticulum (ER) to generate vesicles that are associated with the virus replication complex. The viral protein 6K₂ of turnip mosaic virus (TuMV) is known to induce ER-derived vesicles that contain vRNA as well as viral and host proteins required for vRNA synthesis. These vesicles not only sustain vRNA synthesis, they are also involved in the intercellular trafficking of vRNA. In this investigation, we found that the N-terminal soluble domain of 6K₂ is required for ER export of the protein and for the formation of vesicles. ER export is not absolutely required for vRNA replication but is necessary for virus cell-to-cell movement. Furthermore, we found that 6K₂ physically interacts with the COPII coatomer Sec24a and that an *Arabidopsis thaliana* mutant line with a defective Sec24a shows a delay in the systemic infection by TuMV.

Positive-strand RNA viruses replicate on cellular membranes in order to achieve efficient virus production. These membranous structures have been termed “viral factories” and are associated with virus replication complexes (VRCs) (1, 2). Electron microscopy coupled to tomography has recently been used to get an elaborate three-dimensional view of animal virus-induced membranous structures. For instance, picorna-, corona-, and arteriviruses induce the formation of endoplasmic reticulum (ER)-derived interconnected single- and double-membrane vesicles, cumulating into the formation of a complex meshwork of membranes (3–5). In the case of plant viruses, VRCs are associated with membranous structures that are derived from various organelles, such as the ER, mitochondria, chloroplasts, or peroxisomes (6–9). Host factors, such as RNA-binding proteins, cellular chaperones, and membrane-shaping proteins, are recruited to these sites in support of viral RNA (vRNA) replication (10–12).

One or two viral proteins are responsible for membrane alteration, which concomitantly recruit viral and host factors to form functional VRCs. For example, brome mosaic virus (BMV) RNA replication protein 1a localizes to the ER and induces inward spherule formation into the ER lumen in its yeast (*Saccharomyces cerevisiae*) surrogate host (13). These spherules sequester vRNA template and the viral RNA polymerase 2a. Potato virus X (PVX) triple gene block protein 2 (TGBp2) induces ER-derived granule

formation and cooperates with TGBp1/3 to accomplish virus replication and targeting of the plasmodesmata (PD) (14). The molecular determinants for membrane alteration of several viral proteins have been investigated. In general, these viral proteins contain functional domains for membrane anchorage, protein-protein interactions, and organelle targeting. For red clover necrotic mosaic virus (RCNMV), a stretch of 20 amino acids was identified in the N-terminal region of the auxiliary replicase protein p27 that is sufficient for its membrane association. This domain also contains amino acids that are required for the VRC formation and negative-strand vRNA synthesis (15). The melon

Received 27 February 2015 Accepted 11 April 2015

Accepted manuscript posted online 15 April 2015

Citation Jiang J, Patarroyo C, Garcia Cabanillas D, Zheng H, Laliberté J-F. 2015. The vesicle-forming 6K₂ protein of turnip mosaic virus interacts with the COPII coatomer Sec24a for viral systemic infection. *J Virol* 89:6695–6710. doi:10.1128/JVI.00503-15.

Editor: A. Simon

Address correspondence to Jean-François Laliberté, jean-francois.laliberte@iaf.inrs.ca.

Copyright © 2015, American Society for Microbiology. All Rights Reserved.

doi:10.1128/JVI.00503-15

necrotic spot virus (MNSV) p7B is a type II integral membrane protein, and the short extramembrane N- and C-terminal tails were shown to be essential for ER export and transport to the Golgi apparatus and finally to PDs of the protein (16). Similarly, the C-terminal tail of the bamboo mosaic virus (BaMV) TGBp3 contains a sorting signal that targets infectious viral components to cortical ER for cell-to-cell transmission (17).

Few host factors involved in virus-induced membrane alteration have been identified. For instance, the turnip mosaic virus (TuMV) 6K₂ protein interacts with the SNARE (soluble N-ethylmaleimide-sensitive-factor attachment protein receptor) Vap27 protein, and by binding Vap27, 6K₂ associates also with Syp71: Vap27 and Syp71 are proteins involved in vesicle fusion (18). The p27 auxiliary replication protein of RCNMV, which is needed for the association of the replication complex with ER membranes (15), interacts with the ADP ribosylation factor 1 (Arf1) (19), a small GTPase that is implicated in the formation of the COPI vesicles (20). The p33 replication protein of tomato bushy stunt virus (TBSV) coopts the proteins of the endosomal sorting complexes (ESCRT) that are required for transport of properly assembled VRC on the peroxisome membrane (21, 22). Finally, in yeast, BMV 1a protein interacts with and incorporates reticulons for spherule formation and maintenance of an open channel to the cytoplasm to facilitate import of vRNA templates and export of progeny vRNA (23).

TuMV is a positive sense RNA virus that belongs to the genus *Potyvirus* in the family *Potyviridae* (24). The viral genome, about 9.8 kb in length, is linked covalently to a viral protein known as VPg (virus protein, genome linked) at the 5' terminus and is polyadenylated at the 3' terminus. The single open reading frame (ORF) encodes a 358-kDa polypeptide that is processed by three viral proteinases into at least 11 mature proteins. TuMV infection reorganizes the host cell endomembrane system and blocks protein secretion at the ER-Golgi apparatus interface (25). This reorganization leads to the formation of at least two types of structures: a large perinuclear globular structure and peripheral motile ER-derived vesicles. The perinuclear globular structure is an amalgamation of ER, Golgi bodies, COPII coatomers, and chloroplasts (25) and contains vRNA as well as viral proteins, such as 6K₂, VPg-proteinase, the RNA-dependent RNA polymerase (RdRp), the cytoplasmic inclusion (CI) helicase protein, and host proteins, such as the eukaryotic translation initiation factor (iso)4E [eIF(iso)4E], poly(A)-binding protein (PABP), and eukaryotic translation elongation factor 1A (eEF1A) (26). The perinuclear structure is a collection of numerous 100-nm vesicles and is functionally linked to the peripheral motile ER-derived vesicles (25). These vesicles traffic on transvacuolar strands and actin filaments toward PD and move through these channels to the neighboring cells (26, 27).

The 6-kDa viral protein 6K₂ is responsible for the formation of the vesicles (28). It has been shown that vesicle formation was COPII dependent (25, 29). These studies, however, did not indicate what COPII component is directly interacting with 6K₂ and how mechanistically this involvement takes place. It is also not known if involvement of COPII components is required for vRNA replication *per se* or for intracellular/intercellular movement of the vRNA. In this study, we identified a tryptophan-based motif within the N-terminal cytoplasmic tail of 6K₂ that is necessary for ER export of 6K₂, leading to the formation of viral vesicles and cell-to-cell movement of TuMV. We further showed that 6K₂ in-

teracts with the COPII coatomer Sec24a and that viral systemic spread is reduced in a Sec24a-defective *Arabidopsis thaliana* mutant line. We hypothesize that 6K₂ exits from the ER by interacting with the COPII machinery, and this ER export is necessary for virus intercellular movement to take place.

MATERIALS AND METHODS

Secondary structure prediction of 6K₂. Prediction was done using the following algorithms available online: TMHMM (<http://www.cbs.dtu.dk/services/TMHMM-2.0/>) (30), SOSUI (http://harrier.nagahama-i-bio.ac.jp/sosui/sosui_submit.html) (31), TopPred (<http://mobylye.pasteur.fr/cgi-bin/portal.py?#forms:toppred>) (32), ΔG Prediction Server (<http://dgpred.cbr.su.se/>) (33), MEMSAT (<http://www.sacs.ucsf.edu/cgi-bin/memsat.py>) (34), DAS (<http://www.sbc.su.se/~miklos/DAS/>) (35), PredictProtein (<https://www.predictprotein.org/>) (36), and SPLIT (<http://split4.pmfst.hr/split/4/>) (37). The hydrophobicity index was calculated using MPTOPO (38).

Molecular clones and site-directed mutagenesis. The coding sequences of TuMV 6K₁ and 6K₂ were amplified by PCR using TuMV infectious clone pCambiaTuMV (26) as the template. For construction of pCambia/6K₁:mCherry, the PCR product of 6K₁ was digested with BamHI, followed by ligation with pCambia/mCherry (39), also digested with BamHI. Similar to the steps described above, the PCR product of 6K₂ was digested with XbaI and BamHI and then inserted into vector pCambia/mCherry to generate pCambia/6K₂:mCherry. Mutagenesis was performed using the QuikChange II XL site-directed mutagenesis kit (Agilent), following the manufacturer's instructions. For the pCambia/6K₂:mCherry Δ1–6, Δ1–12, Δ1–18, W15A, K7A, K10A, K12A, K14A, K17A, and K14–17A mutants, pCambia/6K₂:mCherry was used as the template. For mutant pCambiaTuMV^{W15A}, template pCambiaTuMV was used. For mutant pNX32-Sec24a^{R693K}, template pNX32-Sec24a was used. A fragment flanked by KpnI and ApaI from plasmid pCambiaTuMV^{W15A} was used to replace the KpnI/ApaI fragment of vector pCambiaTuMV/6K₂:mCherry (26) and pCambiaTuMV/6K₂:mCherry//GFP-HDEL (25): the resulting constructs were pCambiaTuMV^{W15A}/6K₂:mCherry and pCambiaTuMV^{W15A}/6K₂:mCherry//GFP-HDEL, respectively. The DNA fragment harboring the coding sequence of 6K₂^{W15A}:mCherry flanked by SacII was obtained by PCR using pCambia/6K₂^{W15A}:mCherry as the template. A similar procedure described by Beauchemin et al. (40) was followed to generate pCambiaTuMV^{W15A}/6K₂^{W15A}:mCherry. For construction of pCambia/N₂-TMD₁-C₁:mCherry, two complementary oligonucleotides were annealed. Equal amounts of both oligonucleotides were mixed and heated to 95°C for 2 min and then ramped cool to 25°C over a period of 45 min. The prepared DNA fragment was digested with SalI and then inserted into pCambia/6K₁:mCherry/SalI so that the predicted N-terminal part was replaced with a SalI endonuclease restriction site. All constructs were verified by sequencing.

Protein expression in plants. Transient expression was performed by agroinfiltration on 4-week-old *Nicotiana benthamiana* plants as described previously (41). *Agrobacterium tumefaciens* AGL1 containing a recombinant expression plasmid was selected on LB ampicillin-kanamycin plates, and then cells were cultured overnight. Bacterial cultures were centrifuged and suspended with water solution containing 10 mM MgCl₂ and 150 μM acetosyringone. For expression, the bacterial optical density at 600 nm (OD₆₀₀) was adjusted to 0.03 for green fluorescent protein (GFP)-HDEL (42), 0.1 for yellow fluorescent protein (YFP)-Sec24a (25), and 0.3 for 6K₂ and its mutants. For coexpression, equal volumes of the bacterial suspension were mixed thoroughly. Agroinfiltrated plants were kept in growth chamber for 3 to 5 days until analysis. For brefeldin A (BFA) treatment, 10 μg/ml BFA solution was applied 24 h before observation.

Protoplast isolation and transfection. Protoplast isolation and transfection were performed essentially as Yoo et al. (43). Four-week-old leaves were cut into 1-mm strips and incubated with enzyme solution (1.5% cellulase R10, 0.2% macerozyme R10, 0.4 M mannitol, 20 mM KCl, 20

mM MES [morpholineethanesulfonic acid, pH 5.7], 10 mM CaCl₂, 0.1% bovine serum albumin [BSA]). Vacuum infiltration was applied, and leaves were kept in the dark for 4 h. The enzyme solution was diluted with equal volume of W5 solution (2 mM MES [pH 5.7], 154 mM NaCl, 125 mM CaCl₂, 5 mM KCl) and was filtered with a 41- μ m-pore nylon mesh. The flowthrough was centrifuged at 100 \times g for 3 min. The pellet was resuspended in W5 solution and kept on ice for 30 min. After centrifugation at 100 \times g for 3 min, the W5 solution was removed, and MMg solution (4 mM MES [pH 5.7], 0.4 M mannitol, 15 mM MgCl₂) was added to adjust the protoplast density to 2 \times 10⁶ ml⁻¹. One hundred microliters of protoplast and 10 μ g of expression plasmid were mixed with equal volume of 40% polyethylene glycol (PEG) solution and incubated at room temperature for 20 min. An equal volume of W5 solution was added to stop the transfection. Finally, the protoplasts were resuspended and incubated with W1 solution (4 mM MES [pH 5.7], 0.5 M mannitol, 20 mM KCl) at room temperature for 40 h until analysis.

Cellular fractionation, membrane partitioning, and immunoblotting. The cellular fractionation experiment was performed as described in reference 39. For membrane partitioning, approximately 4 g of leaf tissues expressing 6K₂:mCherry or N₂-TMD₁-C₁:mCherry was homogenized in lysis buffer (20 mM HEPES [pH 6.8], 250 mM mannitol, 150 mM potassium acetate, 1 M MgCl₂). Membrane pellets were obtained as for the cellular fractionation experiment. The pellets were suspended in 10 volumes of 1% Triton X-100, 100 mM Na₂CO₃, 4 M urea, or 1 M KCl and incubated on ice for 30 min. These samples were centrifuged at 30,000 \times g for 30 min to separate the soluble fraction (S30) and the membrane fraction (P30). These fractions were then diluted 5 times for immunoblotting. For immunoblotting, protein samples were analyzed by 12% SDS-PAGE and then transferred to nitrocellulose membrane. Rabbit antisera were used at the following dilutions: anti-CP at 1:2,500 (26), anti-red fluorescent protein (anti-RFP) (Sigma) at 1:10,000, and anti-GFP (Sigma) at 1:10,000. The secondary antibody was horseradish peroxidase-coupled goat anti-rabbit IgG.

Confocal microscopy. Agroinfiltrated leaf sections were imaged using Zeiss LSM780 inverted confocal microscopy with a 20 \times objective and a 40 \times or 63 \times oil immersion objective. Argon and HeNe lasers were used to excite fluorescent proteins, and signals from both green and red channels were collected simultaneously. GFP and YFP were excited at 488 nm, and the emission light was captured at 500 nm to 535 nm; mCherry was excited at 561 nm, and the emission light was captured at 580 nm to 640 nm. Image processing was performed with ZEN 2011 software and Image J.

YTH assay. The yeast two-hybrid (YTH) assay experiments were carried out following the method of Grefen et al. (44). *Saccharomyces cerevisiae* THY-AP4 (*MATa ura3 leu2 lexA::lacZ::trp1 lexA::HIS3 lexA::ADE2*) and THY-AP5 (*MAT α URA3 leu2 trp1 his3 loxP::ade2*) were the yeast strains used. Bait vector pNC-WT-WRC1, allowing an LV-Cub-6K₂ fusion, and prey vector pNX32-DEST, allowing an NubG-prey (proteins of interest) fusion, were utilized to perform pairwise interaction assays of membrane proteins. Yeast transformations were performed using the lithium acetate-based protocol, followed by the mating procedure. The mated colonies carrying both constructs were selected in a synthetic defined medium plus a complete amino acid mix without leucine and tryptophan (SD-LW). To test bait and prey interactions, independent positive-mated colonies were plated for selection both on SD-LW and a synthetic defined medium plus a complete amino acid mix without leucine, tryptophan, and histidine (SD-LWH) plus 3-amino-1,2,4-triazole (3-AT) plus X-Gal (5-bromo-4-chloro-3-indolyl- β -D-galactopyranoside) medium.

Co-IP purification. After agrobacterium-mediated transient expression for 3 days, *N. benthamiana* leaves (approximately 0.3 g) were harvested and ground to powder in liquid nitrogen. Ground tissues were transferred into a tissue homogenizer and mixed with 3.0 ml of immunoprecipitation (IP) buffer (50 mM Tris [pH 7.5], 150 mM NaCl, 10% glycerol, 0.1% Nonidet P-40, 5 mM dithiothreitol, 1 \times Complete protease inhibitor [Roche]). The crude lysates were then centrifuged at 20,000 \times g

TABLE 1 Computer analysis of the TuMV 6K₂ amino acid sequence

Algorithm	Integral membrane protein present	No. of TM segments (starting/ending aa) ^a
TMHMM	Yes	1 (20/39)
SOSUI	Yes	1 (20/42)
TopPred	Yes	1 (22/42)
Δ G Prediction Server	Yes	1 (18/39)
MEMSAT	Yes	1 (24/40)
DAS	Yes	1 (21/39)
PredictProtein	Yes	1 (22/39)
SPLIT	Yes	1 (22/39)

^a aa, amino acid.

for 15 min at 4°C. After centrifugation, 1 ml of the supernatant was incubated with GFP-Trap resin (Chromotek). Elution of the bound proteins was done according to the manufacturer's instructions.

RESULTS

6K₂ is associated with cellular membranes. It has been shown that the TuMV protein 6K₂ is responsible for the production of vesicles that are associated with virus replication and intracellular as well as intercellular movement (26, 27). These vesicles originate from the ER (25, 45). To identify the molecular determinants of TuMV 6K₂ in vesicle biogenesis, secondary structure predictions based on TMHMM, SOSUI, and TopPred, and other algorithms were performed (30, 31, 46). These algorithms predict that 6K₂ is a single-pass integral membrane protein (Table 1). These predictions indicate the presence of a 19-amino-acid N-terminal tail, an 11-amino acid C-terminal tail, and a transmembrane domain (TMD) composed of 23 amino acids (Fig. 1A). These predictions also indicate that 6K₂ has a type II topology. This is exemplified by the TMHMM algorithm, which predicts that the N-terminal tail of 6K₂ is likely located in the cytosol and the C-terminal tail outside (i.e., in the lumen of the ER or inside the vesicle) (Fig. 1B). This prediction is based on the positive-inside rule (47) due to the presence of a lysine-rich region in the predicted N-terminal tail of 6K₂. Beauchemin and Laliberté (45) demonstrated that the VPg-Pro domain of the precursor form 6K₂-VPg-Pro is located in the lumen of 6K₂-induced vesicles, providing experimental support for this prediction.

To confirm experimentally that 6K₂ is a membrane-associated protein, its coding sequence was fused at the 5' end of the coding sequence of the fluorescent protein mCherry in the binary vector pCambia 1380. *N. benthamiana* leaf tissue expressing 6K₂:mCherry was homogenized 3 days after agroinfiltration, and the cellular extract was subjected to low-speed centrifugation to obtain the total protein fraction (S3), which was then separated by high-speed centrifugation into a soluble protein fraction (S30) and a membrane-associated protein fraction (P30). Western blotting using a rabbit serum against mCherry showed the presence of 6K₂:mCherry in the P30 fraction but not in the S30 fraction, indicating that 6K₂ was membrane associated (Fig. 1C). The presence of soluble mCherry in the S30 fraction and of the Golgi apparatus-resident transmembrane protein ST-YFP (48) in the P30 fraction (Fig. 1C) confirmed that the extraction procedure clearly separated soluble from membrane-associated proteins. The 6K₂:mCherry P30 fraction was divided into several aliquots, which were treated with either 1% Triton X-100 to release integral membrane proteins, 100 mM Na₂CO₃ (pH 11) to dislodge proteins

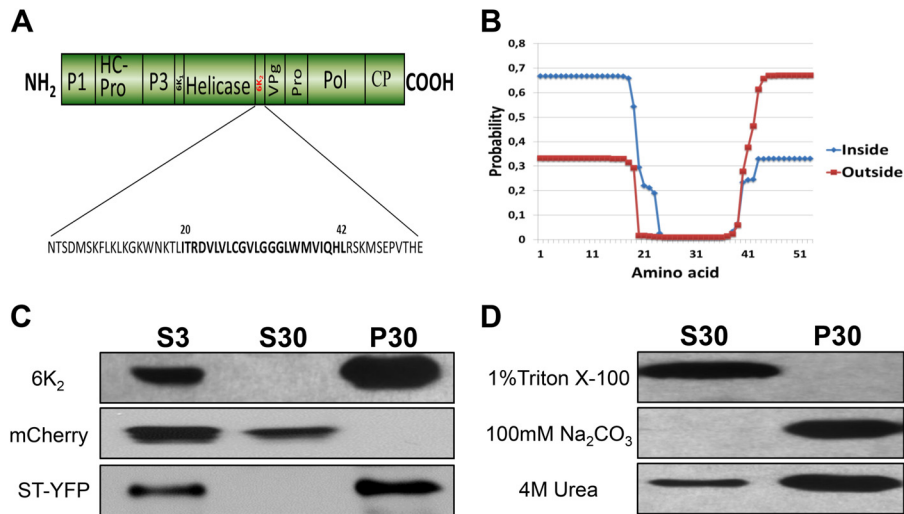


FIG 1 6K₂ is a membrane-associated protein. (A) Schematic representation of the TuMV open reading frames, with 6K₂ highlighted in red. The 6K₂ amino acid sequence is shown below, with the predicted transmembrane domain shown in boldface. (B) 6K₂ topology prediction using the TMHMM server. The probability values of each amino acid residue located inside (shown in blue) and outside (shown in red) are plotted against the corresponding amino acid position. (C) Immunoblot analysis of total, soluble, and membrane-associated proteins of 6K₂:mCherry, mCherry, and ST-YFP. *N. benthamiana* plants were agroinfiltrated with 6K₂:mCherry, mCherry, or ST-YFP and kept in the growth chamber for 3 days. Total proteins (S3) were extracted, and soluble proteins (S30) were separated from membrane-associated proteins (P30) by centrifugation at 30,000 × g. (D) Membrane-enriched fractions of 6K₂:mCherry were treated with 1% Triton X-100, 100 mM Na₂CO₃, or 4 M urea for 30 min at 4°C. After centrifugation, the S30 and P30 fractions were submitted to immunoblot analysis. Proteins were separated by SDS-PAGE and analyzed by Western blotting using a rabbit serum against RFP or GFP.

residing in membrane lumens, or 4 M urea to release peripheral membrane proteins (Fig. 1D). Western blotting showed that Triton X-100 treatment released 6K₂ to the supernatant, while Na₂CO₃ had no effect on membrane association of 6K₂. Urea released some 6K₂ in the S30 fraction, but the viral protein essentially remained associated with the membrane fraction.

The N-terminal tail of 6K₂ renders cytosolic 6K₁ membrane associated. One object of this investigation was to characterize the molecular determinants of 6K₂ for vesicle production. One approach that is often taken is to compare two seemingly similar proteins and look at what is common or different between them that may explain their biological properties. The TuMV genome codes for another viral protein, known as 6K₁, which has the same molecular weight as 6K₂. Secondary structure predictions suggest that 6K₁ is an integral membrane protein, with an N-terminal tail, TMD, and C-terminal tail composed of 3, 20, and 29 amino acids, respectively (Fig. 2A). 6K₁:mCherry, however, was distributed in the cytosol and nucleus (Fig. 2B) and had the same subcellular distribution as soluble mCherry (Fig. 2C). A cellular fractionation experiment was performed, and Western blot analysis showed the presence of 6K₁:mCherry in the S30 fraction but not in the P30 fraction (Fig. 2D), confirming that 6K₁ is a soluble protein when expressed ectopically. The soluble subcellular distribution may be explained by the ΔG_{app} of the TMD of 6K₁ being higher than the one for 6K₂ (ΔG_{app} 6K₁ = 0.749 versus ΔG_{app} 6K₂ = -0.116). ΔG_{app} is defined as the free energy required for the insertion of peptide from water to a lipid environment (38). A negative value for ΔG_{app} indicates that the peptide has a high probability of being recognized as a TMD and integrated into a membrane.

A major difference between the two viral proteins is the predicted length of the N-terminal cytoplasmic tail: the lengths are 3 and 19 residues for 6K₁ and 6K₂, respectively (Fig. 2A versus 1A). The cytoplasmic tails of membrane proteins that enter the early

secretory pathway (ER-Golgi protein transport) often interact with membrane-associated factors—for instance, with the COPII coatomer Sec24a (49). In order to see if the N-terminal cytoplasmic tail of 6K₂ could induce membrane association of 6K₁ through interaction with a membrane-associated host factor(s), the predicted N-terminal tail of 6K₁ was replaced with the N-terminal tail of 6K₂, and the resulting construct was named N₂-TMD₁-C₁ (with the subscript indicating the 6K₁ or 6K₂ origin of the domain) (Fig. 2E). The expression pattern of N₂-TMD₁-C₁:mCherry in *N. benthamiana* cells looked similar to that in cells expressing 6K₁:mCherry or mCherry (Fig. 2F). However, cellular membrane fractionation experiments showed the presence of N₂-TMD₁-C₁:mCherry in the S30 fraction but also in the P30 fraction (Fig. 2G). The P30 fraction was subjected to different chemical treatments, and Western blot analysis showed that treatments with 1 M KCl, 100 mM Na₂CO₃ (pH 11), and 4 M urea released the protein to the supernatant (Fig. 2H). These results indicate that N₂-TMD₁-C₁ is peripherally associated with membranes. It suggests that the 6K₂ N-terminal tail may interact with a host protein that resides in or is peripherally associated with membranes. Interaction with certain lipids is also possible. Alternatively, the addition of the N-terminal tail of 6K₂ to 6K₁ may have induced structural changes within the latter that favored its membrane association.

The N-terminal tail of 6K₂ is required for ER export. Mapping experiments with the purpose of identifying the region in the N-terminal tail that is critical for 6K₂ vesicle formation were thus undertaken. Site-directed mutagenesis was conducted to progressively delete six amino acids of the 6K₂ N-terminal tail, generating 6K₂^{Δ1–6}:mCherry, 6K₂^{Δ1–12}:mCherry, and 6K₂^{Δ1–18}:mCherry (Fig. 3A). Agroinfiltrated *N. benthamiana* epidermal cells expressing the entire 6K₂ fused to mCherry or the truncated 6K₂-fluorescent protein fusions were observed 3 days later. Ectopic expression of 6K₂:mCherry and 6K₂^{Δ1–6}:

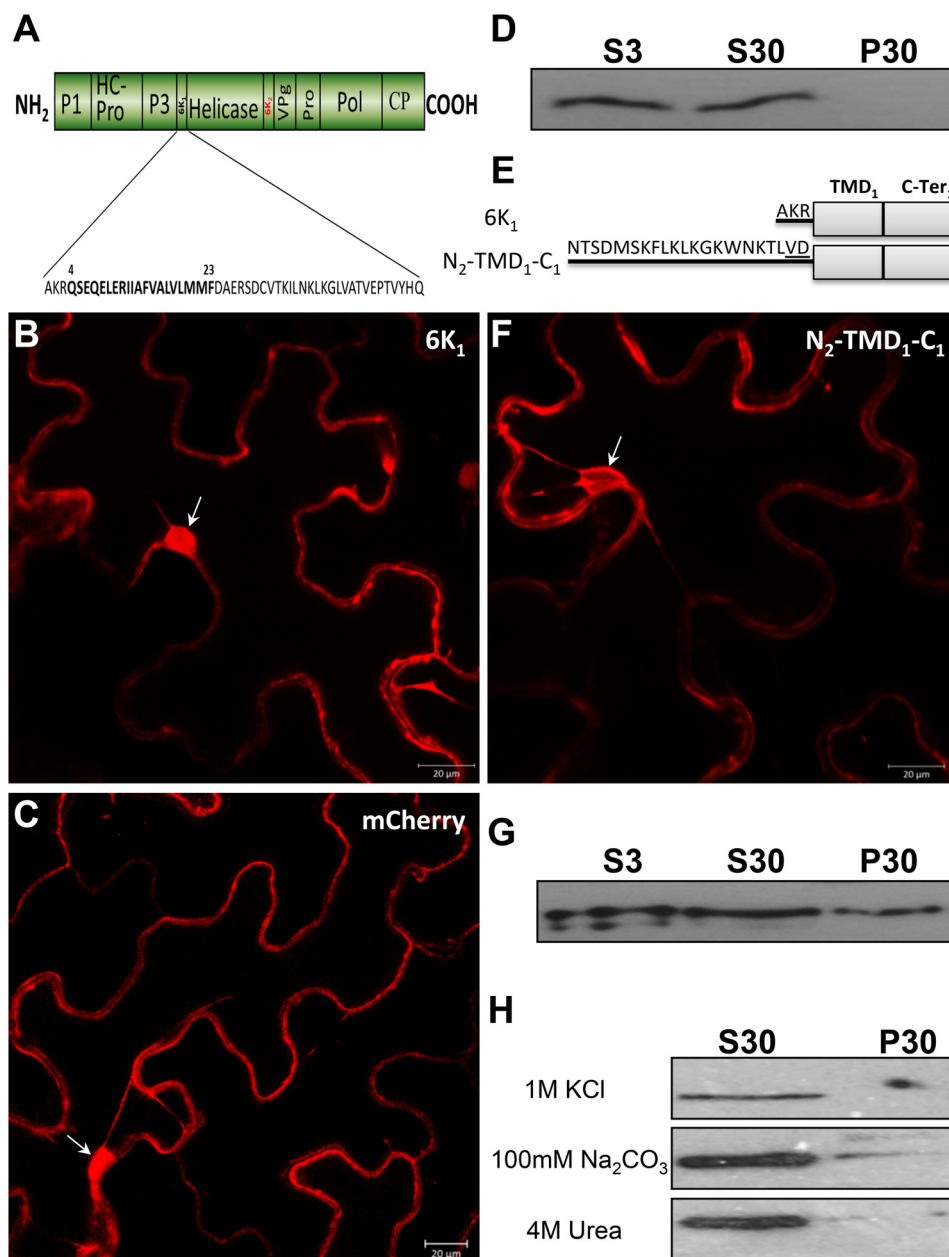


FIG 2 The N-terminal tail of 6K₂ renders cytosolic 6K₁ membrane associated. (A) Protein 6K₁ secondary structure prediction. The 6K₁ amino acid sequence is shown below, and the predicted TMD is shown in boldface. (B and C) Confocal microscopy imaging of leaf epidermal cell of *N. benthamiana* expressing 6K₁:mCherry (B) or mCherry (C) 3 days after agroinfiltration. (D) Fractionation of 6K₁:mCherry total proteins (S3) into soluble (S30) and membrane (P30) fractions and detected by Western blotting. (E) Schematic representation of chimeric protein N₂-TMD₁-C₁ with protein 6K₁ is presented above. Black lines represent the N-terminal portion of each protein, and amino acid residues are shown. The 6K₁ TMD and C-terminal tail are indicated by gray rectangles. Underlined amino acid residues VD are encoded by the incorporated SalI endonuclease restriction site. (F) Confocal microscopy imaging of leaf epidermal cell of *N. benthamiana* expressing N₂-TMD₁-C₁:mCherry 3 days after agroinfiltration. (G and H) *N. benthamiana* leaves expressing N₂-TMD₁-C₁:mCherry and the resulting S3, S30, and P30 were analyzed (G). P30 fractions were incubated with 1 M KCl, 100 mM Na₂CO₃, or 4 M urea, followed by ultracentrifugation and immunoblotting (H). All Western blots were performed with antibodies against RFP. All confocal images are optical images (1- μ m thick). The nucleus is indicated by the white arrow.

mCherry induced the formation of punctate structures that did not significantly colocalize with the ER marker GFP-HDEL (Fig. 3B and C). However, the expression pattern of 6K₂ ^{Δ 1-12}:mCherry (Fig. 3D) and of 6K₂ ^{Δ 1-18}:mCherry (Fig. 3E) was mostly reticulate, and overlapped with the ER marker. The Pearson's correlation coefficient (PCC) *Rr* values, which provide a quantitative estimate

of colocalization (50), were calculated. The PCC *Rr* value for GFP-HDEL with 6K₂:mCherry was 0.04 ± 0.03 , which was not significantly different from the 0.08 ± 0.06 value for GFP-HDEL with 6K₂ ^{Δ 1-6}:mCherry (Fig. 3F). The PCC *Rr* values, however, were significantly higher for GFP-HDEL with 6K₂ ^{Δ 1-12}:mCherry (0.24 ± 0.05) or with 6K₂ ^{Δ 1-18}:mCherry (0.42 ± 0.11), thereby

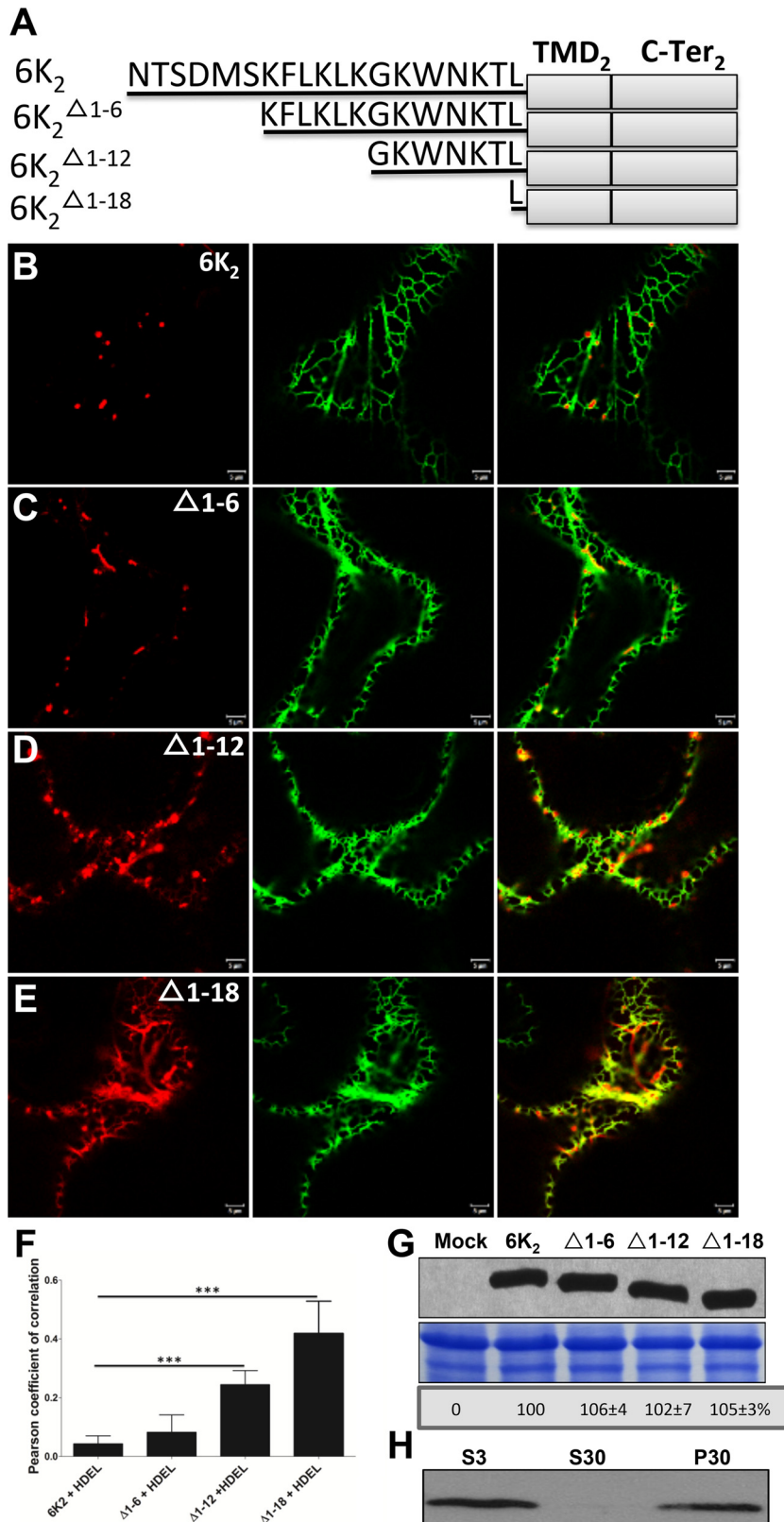


FIG 3 The N-terminal tail is required for ER export of 6K₂. (A) Schematic representation of 6K₂ and truncated 6K₂^{Δ1-6}, 6K₂^{Δ1-12}, and 6K₂^{Δ1-18}. Black lines represent the N-terminal portion of each protein, and amino acid residues are shown. The 6K₂ TMD and C-terminal tail are indicated by gray rectangles. (B to E) Representative *N. benthamiana* epidermal cells coexpressing 6K₂:mCherry (B), 6K₂^{Δ1-6}:mCherry (C), 6K₂^{Δ1-12}:mCherry (D), or 6K₂^{Δ1-18}:mCherry (E) with ER marker GFP-HDEL were imaged using confocal microscopy. These images are optical images (1-μm thick). (F) Colocalization statistical analysis between GFP-HDEL and the WT or the truncated 6K₂ vesicles by calculation of the Pearson's correlation coefficient *Rr* values. Significant difference (Student's *t* tests, *P* < 0.001) is indicated by asterisks. Mean values ± standard deviations (SD) from three independent experiments are shown. (G) WT 6K₂:mCherry and its N-terminal truncations detected by Western blotting. The bottom panels show equal loading verified by Coomassie staining. (H) Immunoblot analysis of the S3, S30, and P30 fractions of 6K₂^{Δ1-18}:mCherry. All Western blots were performed with antibodies raised against RFP.

confirming the increasing retention of the latter two deletion mutants in the ER. The reticulate pattern of 6K₂^{Δ1–12}:mCherry and of 6K₂^{Δ1–18}:mCherry was not the result of higher expression than that of 6K₂:mCherry and 6K₂^{Δ1–6}:mCherry since Western blot analysis showed that the expression level of the truncated 6K₂ proteins was similar to that of wild-type (WT) 6K₂ (Fig. 3G). Cellular fractionation experiments followed by Western blotting showed that 6K₂^{Δ1–18}:mCherry was found in the P30 fraction, indicating that this deletion mutant was still membrane associated (Fig. 3H). In conclusion, progressive deletion of the N-terminal tail led to 6K₂ retention in the ER. These results indicate that the N-terminal tail contains amino acids that are important for 6K₂ vesicle formation from the ER. These amino acids are likely located between residues 7 and 18 in the N-terminal tail of 6K₂.

A conserved tryptophan residue and two lysine residues in the N-terminal tail of 6K₂ are important for ER export. In order to pinpoint amino acids important for ER export, we compared different potyvirus 6K₂ N-terminal tail amino acid sequences. Sequence alignment revealed several highly conserved lysine and tryptophan residues between residues 7 and 18 (Fig. 4A). Dibasic motifs have been shown to be involved in protein ER export (51, 52), and the 6K₂ N-terminal tail contains many lysine residues. The resulting single point mutants 6K₂^{K7A}, 6K₂^{K10A}, 6K₂^{K12A}, 6K₂^{K14A}, and 6K₂^{K17A} were produced and expressed as mCherry fusions in *N. benthamiana*. All expression of these mutants induced punctate structures (data not shown) similar to those observed with wild-type 6K₂:mCherry (Fig. 4B). However, when K14 and K17 were simultaneously replaced with alanine, the resulting double mutant (6K₂^{K14A-K17A}) still produced punctate structures but was also partially retained in the ER (Fig. 4C). The highly conserved tryptophan residue was also substituted for alanine, and the mutant (6K₂^{W15A}) protein was expressed in *N. benthamiana*. Even though expression of 6K₂^{W15A}:mCherry induced the formation of punctate structures, ER retention was observed (Fig. 4D). Thus, the 6K₂^{K14A-K17A} and 6K₂^{W15A} mutations did not lead to complete ER retention but rather slowed down ER export of the viral protein. The PCC *Rr* value for GFP-HDEL with 6K₂^{K14A-K17A}:mCherry was 0.22 ± 0.03, and with 6K₂^{W15A}:mCherry was 0.32 ± 0.04, values that were significantly higher than with 6K₂:mCherry (0.04 ± 0.03) (Fig. 4E). We verified that the modified expression pattern was not a result of differential 6K₂ protein expression levels. Western blot analysis showed that 6K₂^{K14A-K17A} and 6K₂^{W15A} were expressed at similar levels to 6K₂ (Fig. 4F). In conclusion, the tryptophan residue at position 15 and the lysine residues at position 14 and 17 are involved in 6K₂ export from the ER.

Tryptophan residue is required for TuMV systemic movement. The above-described experiments indicated that the tryptophan residue located at position 15 in the N-terminal tail of 6K₂ is important for ER export of the viral protein. We consequently introduced this mutation into an infectious viral clone (TuMV^{W15A}) to test its impact on virus infection. As a negative control, the core GDD motif of the viral RdRp was mutated to VNN (TuMV^{VNN}) to produce a replication-defective virus (53). The mock virus, TuMV, TuMV^{W15A}, and TuMV^{VNN} were agroinoculated in *N. benthamiana* plant leaf tissues. At 5 days postinfection (dpi), plants infected with TuMV showed significant growth stunting, while plants infected with TuMV^{W15A} were similar to mock-infected plants (data not shown). Virus production was analyzed by immunoblotting using a rabbit serum against CP (26). Figure 5A shows a high level of CP production for TuMV and

a faint accumulation for TuMV^{VNN} in agroinfiltrated leaves. Agroinfiltration with TuMV^{W15A} showed an ~60% reduction in CP production, indicating it was replication competent even though it did not reach as high a level as wild-type TuMV. CP production was also assessed 40 h later following transfection of *N. benthamiana* protoplasts with mock virus or p35STuMV^{VNN}, p35STuMV^{W15A}, and p35STuMV by Western blotting. Figure 5B shows that p35STuMV^{W15A} produced less CP than WT TuMV, suggesting that viral RNA replication was affected by the mutation. Systemic virus movement in upper nonagroinfiltrated leaves was also evaluated by Western blotting. A strong CP signal was detected in TuMV-infected plants, while no CP was observed for TuMV^{W15A} and TuMV^{VNN} at 5 dpi (Fig. 5C). Furthermore, no CP was detected when Western analysis was performed 2 weeks later (data not shown), even though TuMV^{W15A} replicated at half the level of WT TuMV according to the protoplast experiment. In conclusion, the replacement of tryptophan 15 of 6K₂ with an alanine residue affected cellular virus replication and virus systemic movement.

TuMV^{W15A} replication but not virus intercellular movement is partially complemented by *cis* expression of 6K₂. The W15A mutation reduced virus production in protoplasts and inoculated leaves and prevented plant systemic infection. We then designed an experiment to explore whether TuMV^{W15A} replication and/or movement could be *cis*-complemented by expression of WT 6K₂. We constructed modified infectious clones TuMV^{W15A}/6K₂^{W15A}:mCherry and TuMV^{W15A}/6K₂:mCherry, in which 6K₂^{W15A}:mCherry and 6K₂:mCherry coding sequences were inserted between the P1 and HC-Pro coding sequences in the TuMV^{W15A} backbone, respectively (Fig. 6A). *N. benthamiana* epidermal cells were then agroinfiltrated with the constructs described above, and Western blot analysis was performed with the anti-CP serum. A larger amount of CP accumulation was detected for TuMV^{W15A}/6K₂:mCherry than for TuMV^{W15A}/6K₂^{W15A}:mCherry, but less than for TuMV/6K₂:mCherry (Fig. 6B). This experiment indicates that TuMV^{W15A} replication could be partially complemented by WT 6K₂ when expressed in *cis*.

We next tested if WT 6K₂ could complement the W15A mutation for cell-to-cell movement. We used a plasmid that contained an expression cassette for TuMV tagged with 6K₂:mCherry and another expression cassette for GFP-HDEL, both under the control of the CaMV 35S promoter and within the left and right border sequences of the transfer DNA (T-DNA) (designated TuMV/6K₂:mCherry//GFP-HDEL) (Fig. 6A). With this dual cassette construct, we showed that we can distinguish primary infection foci when cells express both mCherry and GFP from secondary infection foci when cells express mCherry alone (54). We replaced the tryptophan with alanine of the endogenous 6K₂, and the resulting construct was designated TuMV^{W15A}/6K₂:mCherry//GFP-HDEL (Fig. 6A). Agroinfiltrated leaves were examined 5 days later by confocal microscopy with a 20× objective. As expected, TuMV expressing 6K₂:mCherry could move beyond the primary infected cells (Fig. 6C), while TuMV^{W15A} was restricted exclusively to the primary infection foci (Fig. 6D). Almost every TuMV-infected cell sample analyzed (*n* = 45) showed several cell layers of virus movement, while no movement was observed for TuMV^{W15A}-infected cell samples (*n* = 40) (Fig. 6E). These results indicate that virus cell-to-cell movement cannot be complemented by WT 6K₂ expressed in *cis*. Possibly, 6K₂^{W15A} acts as a dominant-negative mutant that affects WT 6K₂ function.

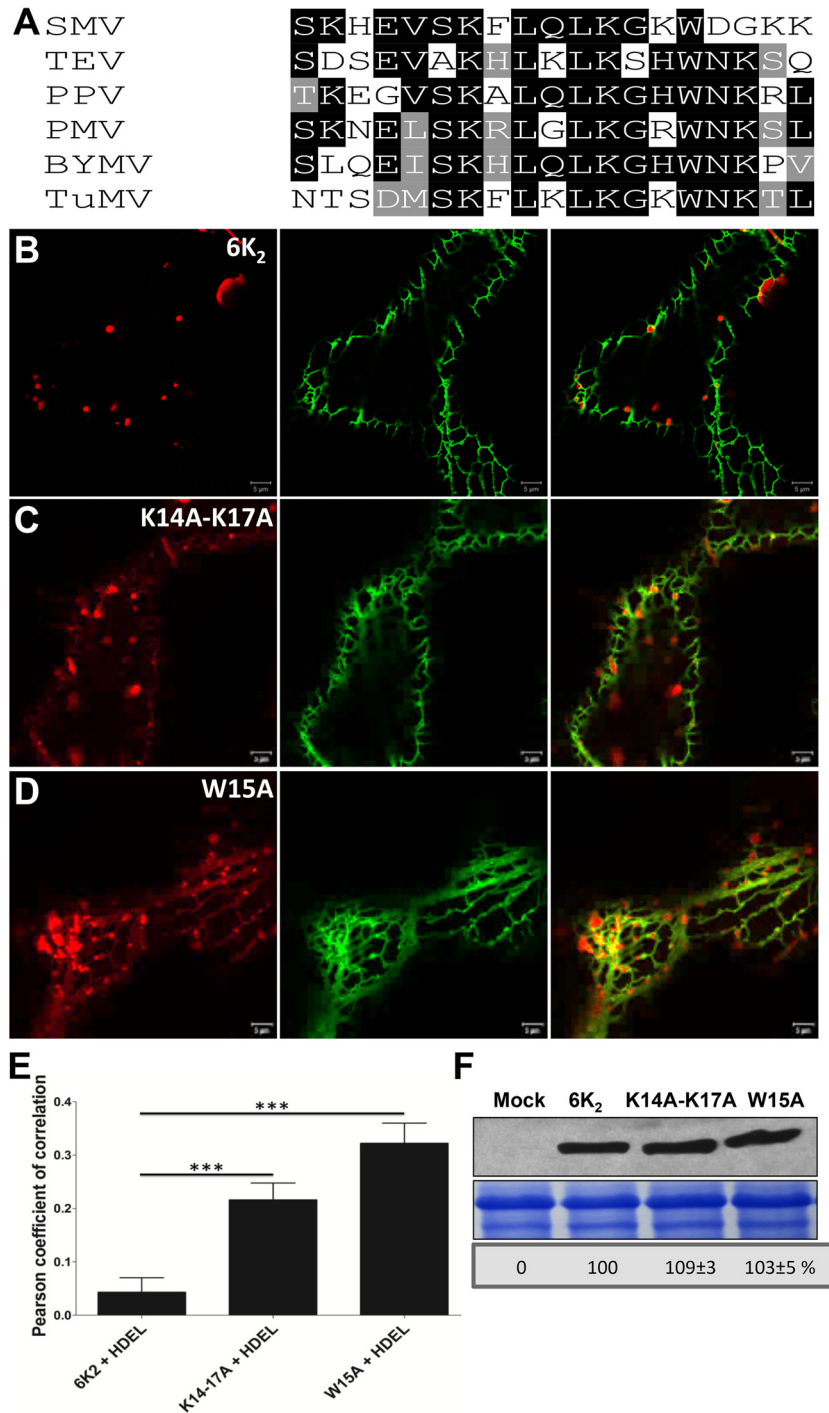


FIG 4 A conserved tryptophan residue and two lysine residues are important for 6K₂ ER export. (A) BLAST of predicted potyviral 6K₂ N-terminal tail amino acid sequences. SMV, soybean mosaic virus; TEV, tobacco etch virus; PPV, plum pox virus; PMV, peanut mottle virus; BYMV, bean yellow mosaic virus; TuMV, turnip mosaic virus. Identical amino acid residues that are highly conserved are highlighted by black boxes, and similar amino acid residues are indicated by gray boxes. (B to D) Confocal images of *N. benthamiana* epidermal cells coexpressing WT 6K₂ (B), 6K₂^{K14A-K17A} (C), or 6K₂^{W15A} (D) with the ER marker GFP-HDEL. These images are optical images (1 μm thick). (E) Colocalization statistical analysis between GFP-HDEL and the WT or the mutated 6K₂ vesicles by calculation of the Pearson's correlation coefficient *Rr* values. Significant difference (Student's *t* tests, *P* < 0.001) is indicated by asterisks. Mean values ± SD from three independent experiments are shown. (F) WT 6K₂:mCherry, 6K₂^{K14A-K17A}:mCherry, and 6K₂^{W15A}:mCherry detected by Western blotting with antibodies raised against RFP. The bottom panels show equal loading verified by Coomassie staining.

6K₂ colocalizes and interacts with the COPII coatmer Sec24a. 6K₂ vesicles use the secretory pathway through the Golgi apparatus to reach PD from the ER (27, 54), and COPII vesicular trafficking has been shown to be involved in 6K₂ intracellular

movement (25, 29). COPII vesicle formation involves the guanine nucleotide exchange factor Sec12, which recruits GTPase Sar1 to ER export sites (ERES), which then interact with Sec23-Sec24 and Sec13-Sec31 complexes to initiate vesicular transport involved in

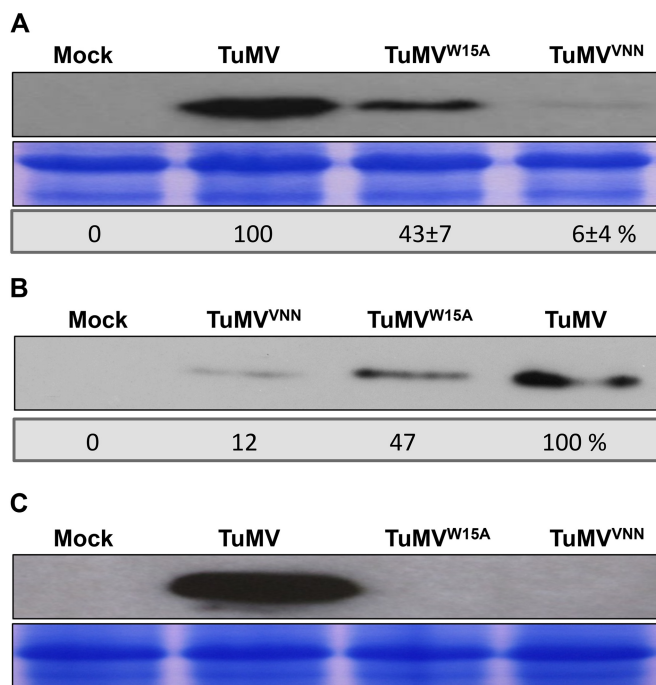


FIG 5 The tryptophan residue is required for TuMV systemic movement. (A) Agroinfiltrated leaves of mock-infected or TuMV-, TuMV^{W15A}-, and TuMV^{VNN}-infected *N. benthamiana* were evaluated by Western blotting 5 days later. (B) *N. benthamiana* protoplasts were mock transfected or transfected with p35STuMV^{VNN}, p35STuMV^{W15A}, and CP was detected by Western blotting 40 h after transfection. (C) The upper nonagroinfiltrated leaves from panel A were analyzed by Western blotting. The bottom panels in panels A and C show equal protein loading verified by Coomassie-staining. All immunoblotting was performed with anti-TuMV CP rabbit serum.

protein ER export (20). Sec24 is the factor that interacts with cargo proteins for their ER-to-Golgi apparatus vesicular transport. The *Arabidopsis* genome encodes three Sec24 homologs (Sec24a, Sec24b, and Sec24c). *A. thaliana* Sec24a (AtSec24a) has been shown to be involved in protein COPII-dependent ER-Golgi apparatus transport (20), while AtSec24b and AtSec24c may have a similar cellular function that is essential in male and female gametogenesis (55).

To verify if 6K₂ ER export may involve interaction with Sec24a, we first check for colocalization between the two proteins. We expressed the COPII marker YFP-Sec24a (25) in leaves infected with TuMV/6K₂:mCherry. Partial colocalization was found with YFP-Sec24a and 6K₂:mCherry (Fig. 7A). This partial colocalization likely reflects the dynamic nature of 6K₂, which is expected to leave COPII vesicles upon entry in the Golgi apparatus (54). Blocking of ER-to-Golgi trafficking should consequently increase the colocalization between the two proteins. We consequently treated cells infected with TuMV/6K₂:mCherry and expressing YFP-Sec24a with BFA, an antibiotic that inhibits protein retrieval from the Golgi apparatus to the ER (56). Figure 7B shows that there was near complete colocalization of 6K₂ vesicles with Sec24a in the presence of BFA. The PCC *Rr* value for the perfectly colocalized *cis*-Golgi markers ERD2:GFP with Man49:mCherry (25) was 0.69 ± 0.05 (Fig. 7C). The PCC *Rr* value for Sec24a with 6K₂ in the absence of BFA was 0.10 ± 0.02, but it was significantly higher in the presence of BFA (0.32 ± 0.03). This outcome is

similar to what has been observed previously (25). This indicates that when ER-to-Golgi trafficking is perturbed, 6K₂ vesicles localize more frequently with Sec24a.

We next carried out a yeast-two-hybrid (YTH) assay to test whether 6K₂ is able to interact with Sec24a. As 6K₂ is a membrane protein, we used the split-ubiquitin membrane-based YTH system that is optimized for membrane protein interaction assay. Cotransformation of LV-Cub-6K₂ with the empty vector NubG indicated that 6K₂ did not autoactivate the system (see Fig. 8A). We used LV-Cub-6K₂ and NubG-6K₂ as positive interaction controls, since 6K₂-6K₂ interaction was demonstrated by bimolecular fluorescence (BiFC) and co-IP experiments (data not shown). We next tested the interaction of LV-Cub-6K₂ with NubG-Sar1 or NubG-Sec24a. Our results showed that 6K₂ interacted with Sec24a but not with Sar1 (Fig. 8A). Although it cannot be excluded, reporter gene activation by Sec24a alone is not likely since interaction between Sec24a and 6K₂ was subsequently confirmed by co-IP experiments (see below).

To further confirm this YTH interaction, 6K₂:mCherry and YFP-Sec24a fusion proteins were transiently expressed in *N. benthamiana* leaves, and interaction was assayed by coimmunoprecipitation of YFP-Sec24a. As shown in Fig. 8B, 6K₂:mCherry was copurified along with YFP-Sec24a. Samples coexpressing control mCherry with YFP, mCherry with YFP-Sec24a, or 6K₂:mCherry with YFP did not show any copurification. These results indicate that 6K₂ interacts with Sec24a. To confirm that the N-terminal cytoplasmic tail of 6K₂ was responsible for Sec24a binding, we tested if N₂-TMD₁-C₁ could bind Sec24a. The co-IP experiment indicated that indeed N₂-TMD₁-C₁:mCherry was purified along with YFP-Sec24a but not 6K₂:mCherry (Fig. 8C). In conclusion, these results showed that 6K₂ interacts with Sec24a and that the N-terminal predicted cytoplasmic tail is involved in the binding.

Defective Sec24a slows down TuMV systemic movement. We then verified the impact of a modified Sec24a for TuMV infection. Since homozygous *A. thaliana* knockout mutant for Sec24a cannot be generated, the importance of Sec24a in TuMV systemic movement was evaluated by infecting the *A. thaliana* *g92* mutant line (57) with TuMV/6K₂:GFP. The *g92* mutant line has a missense mutation in the gene coding for Sec24a that causes conversion of an Arg residue at position 693 to a Lys residue (Sec24a^{R693K}) in a region considered important for cargo binding. This partial loss of function of Sec24a induces the accumulation of Golgi bodies in globular structures composed of a mass of convoluted ER, similar to what is observed during TuMV infection. We first tested if Sec24a^{R693K} could interact with 6K₂ by YTH assay, and no growth on selective medium was observed (Fig. 9A). We then infected *A. thaliana* with TuMV/6K₂:GFP and noticed that wild-type *A. thaliana* was systemically infected at 11 dpi, while the *g92* mutant was not (Fig. 9B). Western blot analysis using a rabbit serum against CP confirmed virus accumulation in the upper noninoculated leaves of wild-type *A. thaliana* but not the *g92* mutant (Fig. 9C). We repeated this experiment three times by infecting 16 plants and scored for systemic infection by UV light evaluation at 11 and 13 dpi. On average, we found that 80% of WT *Arabidopsis* Columbia-0 plants showed systemic infection, while less than 10% of *g92* plants were systemically infected at 11 dpi (Table 2). At 13 dpi, ~40% of *g92* plants were systemically infected. To assess virus replication at the cellular level, we isolated protoplasts from WT and *g92* *A. thaliana* plants, and each proto-

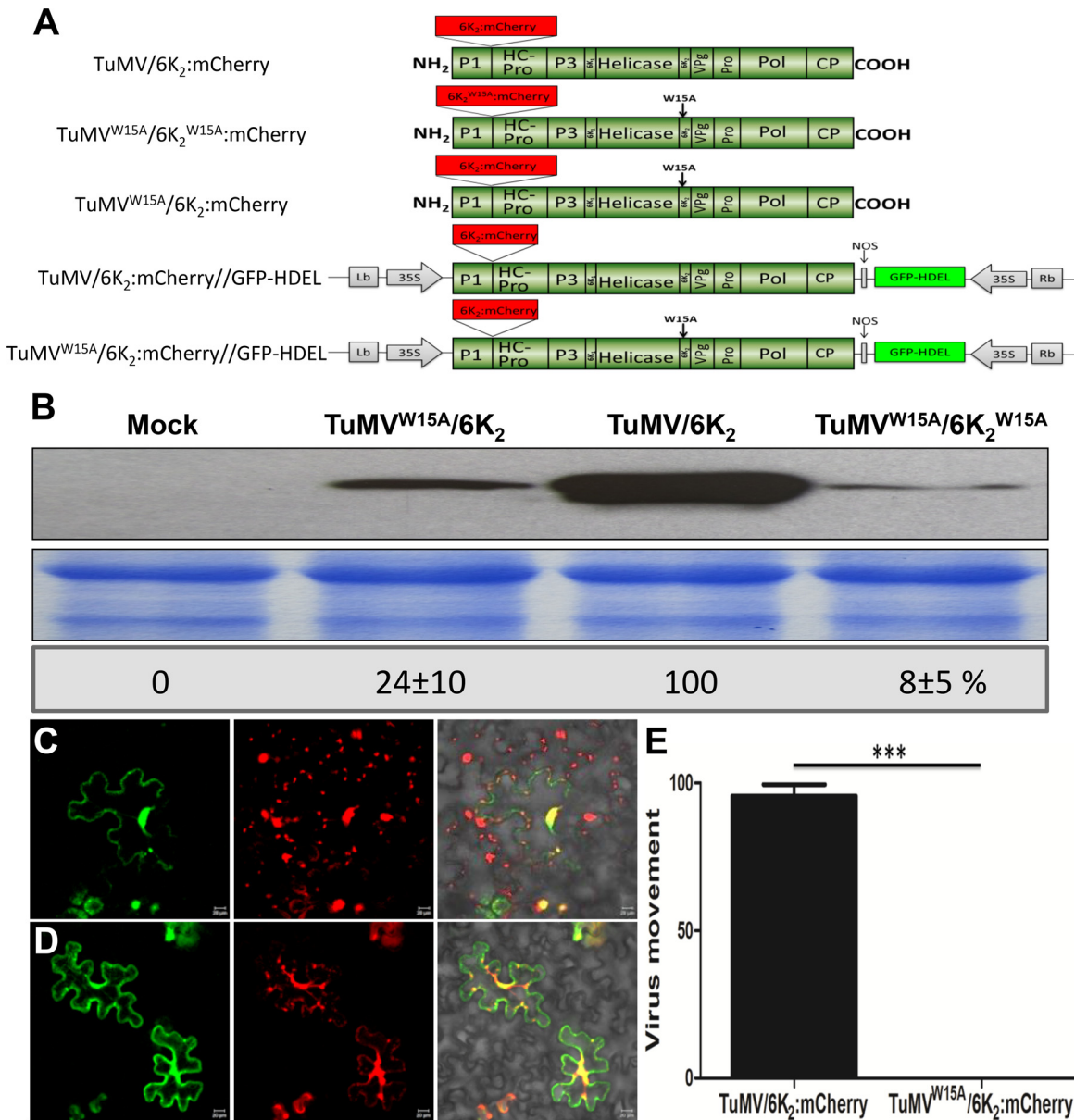


FIG 6 TuMV^{W15A} replication but not virus movement is complemented by *cis* expression of wild-type 6K₂. (A) Schematic representation of TuMV/6K₂:mCherry, TuMV^{W15A}/6K₂^{W15A}:mCherry, TuMV^{W15A}/6K₂:mCherry, TuMV/6K₂:mCherry//GFP-HDEL, and TuMV^{W15A}/6K₂:mCherry//GFP-HDEL. One copy of 6K₂ (wild type or mutated) between P1 and HC-Pro is shown as a red box. Endogenous 6K₂ is located between the helicase and VPg, and the W15A mutation is indicated by an arrow. Gray rectangles represent the left and right borders of T-DNA, and gray arrows represent the CaMV 35S promoter. (B) Detection of CP accumulation in leaves mock infected or infected with TuMV^{W15A}/6K₂:mCherry, TuMV/6K₂:mCherry, and TuMV^{W15A}/6K₂^{W15A}:mCherry with anti-TuMV CP serum. Coomassie blue staining (bottom panel) shows equal protein loading. (C and D) Confocal images of *N. benthamiana* epidermal cells infected with TuMV/6K₂:mCherry//GFP-HDEL (C) and TuMV^{W15A}/6K₂:mCherry//GFP-HDEL (D). Optical images (2 μm thick) of green, red, and merged colors are shown. (E) Statistical analysis of the percentage of virus cell-to-cell movement of TuMV/6K₂:mCherry//GFP-HDEL and TuMV^{W15A}/6K₂:mCherry//GFP-HDEL infection foci. Significant differences (Student's *t* tests, *P* < 0.001) are indicated by asterisks. Mean values ± SD from three independent experiments are shown.

plast preparation was split into three aliquots and mock transfected or transfected with p35STuMV^{VNN} and p35STuMV, respectively. After an incubation period of 40 h, CP production was assessed by immunoblot analysis. Since protein loading may differ between the WT and g92 protoplast preparations, the CP level for the p35STuMV^{VNN} samples was given a score of 1×. CP quantification for the p35STuMV of WT and g92 protoplast samples was normalized accordingly. We found that TuMV replication levels

were similar in both plants (Fig. 9D). We also agroinfiltrated WT and g92 *A. thaliana* leaves with TuMV/6K₂:mCherry//GFP-HDEL to assess intercellular movement of TuMV. At 8 dpi, red-only fluorescence zones, indicative of virus intercellular movement, were clearly observed in WT *A. thaliana*, while this was not the case for g92 plants (Fig. 9E versus F). Intercellular movement was, however, detected for both plants at 12 dpi. This indicates that the g92 mutant line does not compromise TuMV cellular production,

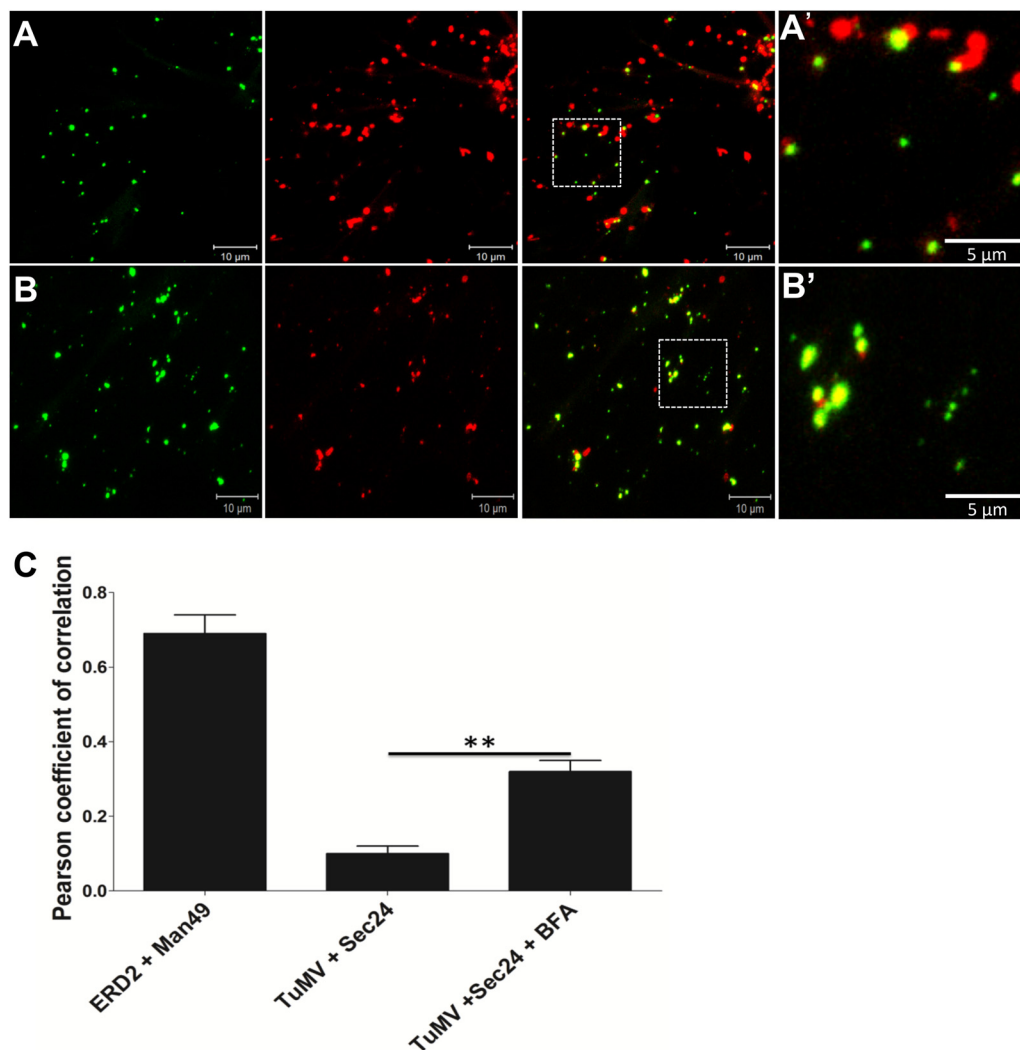


FIG 7 6K₂ colocalizes with COPII coatomer Sec24a. (A and B) *N. benthamiana* cells coexpressing YFP-Sec24a (left panel) with TuMV/6K₂:mCherry (middle panel) in the absence (A) and presence (B) of BFA, with merged panels shown on the right. The area in the dashed box in panels A and B is shown on the right in panels A' and B', respectively. (C) Colocalization statistical analysis between YFP-Sec24a and the 6K₂-mCherry-tagged vesicles by calculation of the Pearson's correlation coefficient *Rr* values. *Rr* values for two colocalizing proteins, ERD2:GFP and Man49:mCherry, are given. For statistical analysis of TuMV/6K₂:mCherry plus Sec24a and TuMV/6K₂:mCherry plus Sec24a plus BFA colocalization, the sample number (*n*) is 26 for each tested combination. Significant differences (Student's *t* tests, 0.001 < *P* < 0.01) are indicated by asterisks. Mean values ± SD from three independent experiments are shown.

but the presence of a defective Sec24a slows down the systemic movement of TuMV.

DISCUSSION

TuMV 6K₂-induced vesicles have been shown to traffic through the secretory pathway for successful viral infection (25–27, 54). Additionally, 6K₂-induced vesicles of TEV were found at ERES, and their formation was shown to be dependent on COPI and COPII factors (29, 58). These studies, however, did not provide a mechanistic explanation on how 6K₂ is involved with the COPII machinery and what COPII component is directly interacting with 6K₂. It is also not known if involvement of COPII components is required for vRNA replication *per se* or for cellular movement of the vRNA.

Secondary structure predictions indicated that 6K₂ is an integral membrane protein (Table 1). According to these predictions,

the C-terminal end would be located in the lumen of the 6K₂ vesicles. This is supported by prior studies demonstrating that the VPg-Pro domain of the precursor form 6K₂-VPg-Pro is located in the lumen of 6K₂-induced vesicles (28) and that PABP, which interacts with VPg, is internalized in the same vesicles (45). The observation, however, that some 6K₂ was released from the P30 fraction upon treatment with urea (Fig. 1) suggests that the viral protein may not be an integral membrane protein but rather is tightly associated with cellular membranes. Treatment with urea was also shown to release the tobacco mosaic virus 30K movement protein from membranes and was concluded to be peripherally associated with cellular membranes (59). Consequently, we cannot definitely conclude that 6K₂ is an integral membrane protein. Experiments involving proteolytic protection and bimolecular fluorescence complementation assays will be needed to solve this issue.

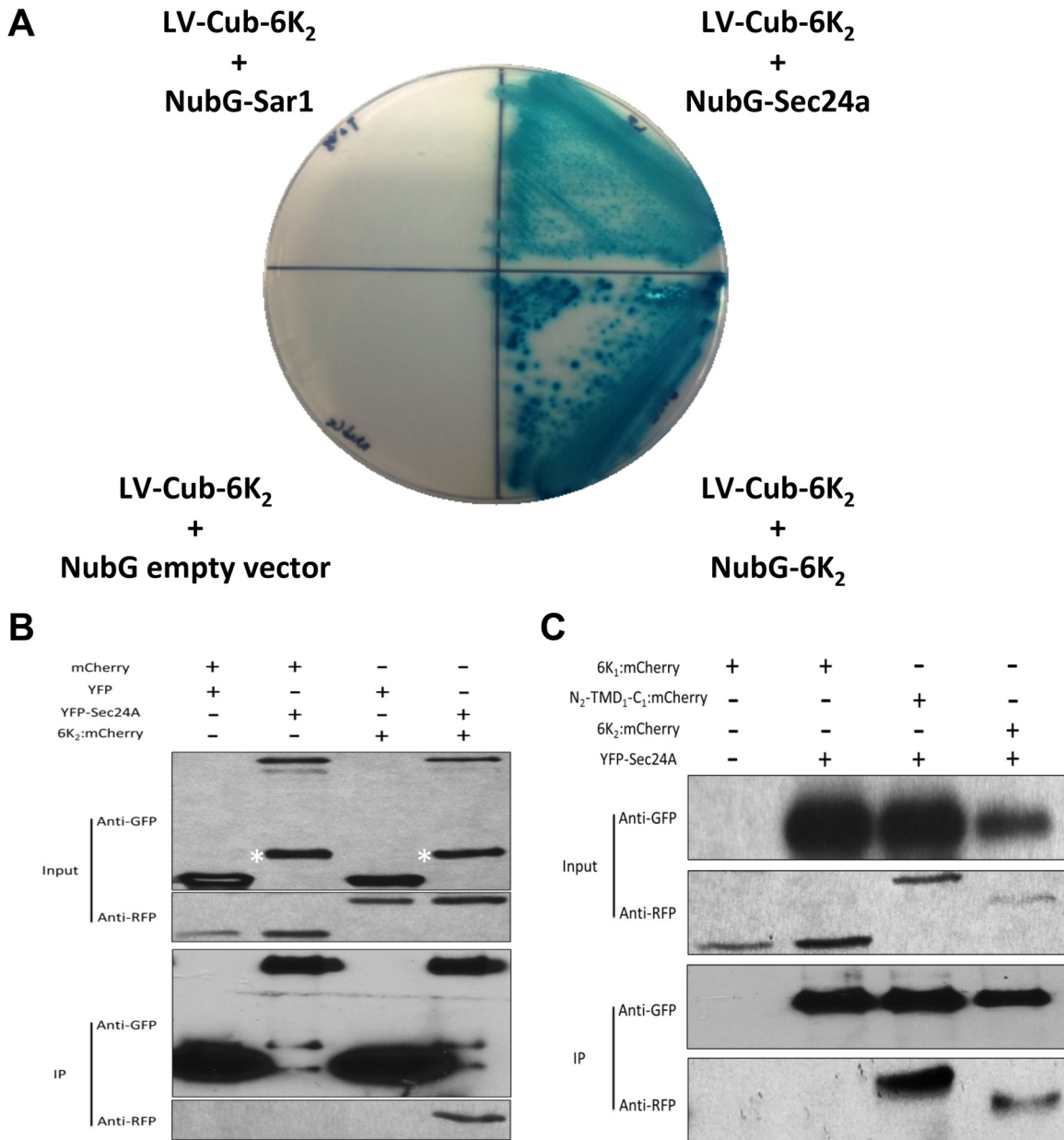


FIG 8 6K₂ interacts with COPII coatomer Sec24a. (A) Yeast two-hybrid assay for protein-protein interactions of TuMV 6K₂ with Sar1 and Sec24a. The transformants were plated on an SD - Leu - Trp - His plus X-Gal plus 3-AT medium. (Upper left) 6K₂ plus Sar1 (LV-Cub-6K₂ plus NubG-Sar1). (Upper right) 6K₂ plus Sec24a (LV-Cub-6K₂ plus NubG-Sec24a). (Lower left) Negative control (LV-Cub-6K₂ plus NubG empty vector). (Lower right) Positive control (LV-Cub-6K₂ plus NubG-6K₂). (B) *N. benthamiana* leaves expressing combinations of mCherry and YFP, mCherry and YFP-Sec24a, YFP and 6K₂:mCherry, or YFP-Sec24a and 6K₂:mCherry were harvested 3 days after agroinfiltration. The cleared lysates (input) were subjected to immunopurification on a GFP-Trap resin, followed by Western blot analysis of input and immunopurified (IP) fractions using antibodies against GFP and RFP. The asterisk indicates a nonspecific or a degradation protein species recognized by the anti-GFP serum. (C) *N. benthamiana* leaves expressing 6K₁:mCherry alone, 6K₁:mCherry and YFP-Sec24a, N₂-TMD₁-C₁:mCherry and YFP-Sec24a, and 6K₂:mCherry and YFP-Sec24a were analyzed as described for panel B.

6K₂ normally induces the formation of motile vesicles that contain replication complexes (26). In the present study, we found that 6K₂ was retained in the ER, with fewer vesicles being formed when the N-terminal 18 amino acids were deleted (Fig. 3). This indicated that this region contained a motif or motifs for the ER export of the viral protein. We further defined the motif(s) by showing that changing the tryptophan residue at position 15 or both lysine residues at positions 14 and 17 into alanine residues resulted in partial ER retention of the protein (Fig. 4). This indi-

cated that these amino acid residues are nonredundant in ER export, suggesting the presence of a combinatorial ER export motif, which might be required to ensure a tight interaction with COPII vesicles (60). ER export motifs for many proteins that undergo ER-Golgi apparatus transport have been identified. Those ER export motifs can be divided into four types: diacidic (DXE, EXXD, and YXΦESDG [where X is any amino acid and Φ is a bulky, hydrophobic residue]), dibasic [(RK)X(RK)], dihydrophobic (LL, LxL, and VV), and diaromatic (FF, YY, or FY) motifs (49). In the

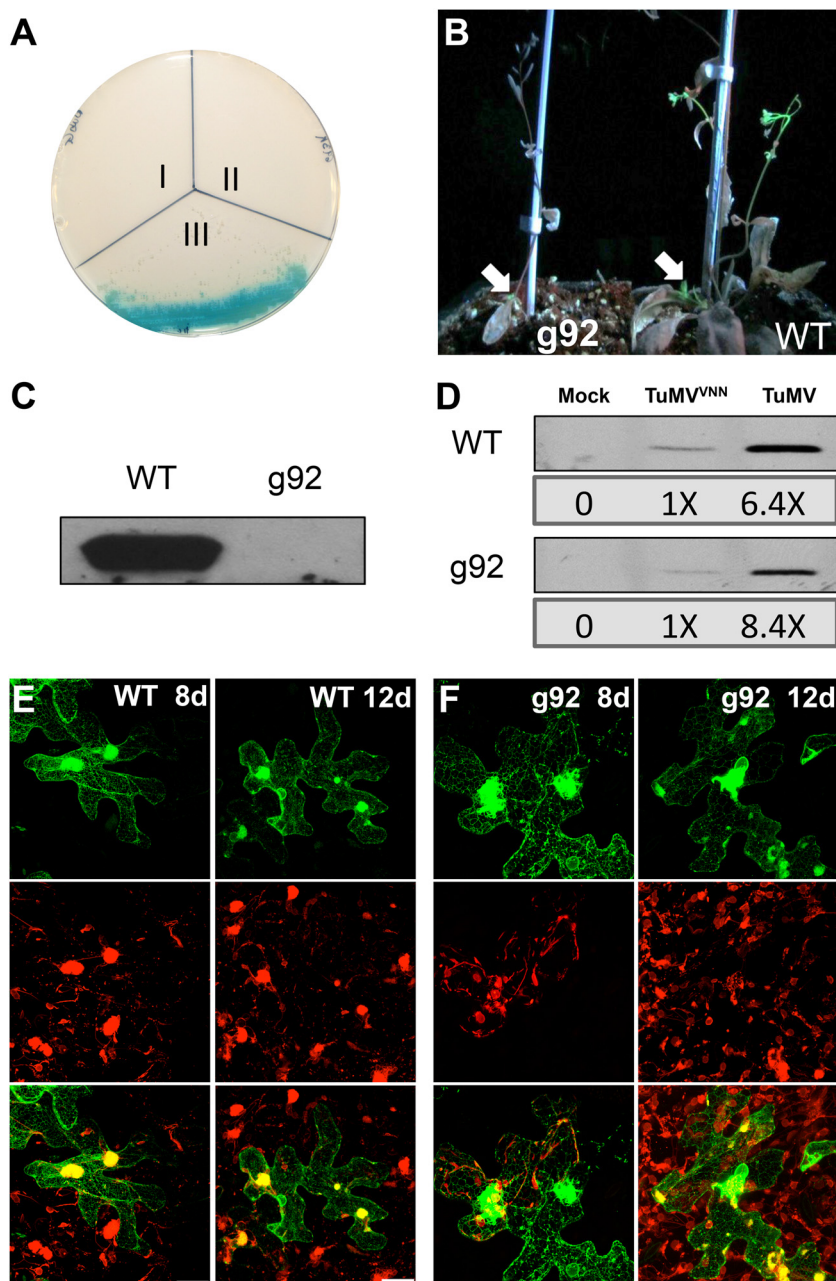


FIG 9 Infection of *g92 Arabidopsis thaliana*. (A) Yeast two-hybrid assay for protein-protein interactions of TuMV 6K₂ with Sec24a^{R693K}. The transformants were plated on an SD -Leu -Trp -His plus X-Gal plus 3-AT medium. I, negative control (LV-Cub-6K2 plus NubG empty vector); II, 6K₂ plus Sec24a^{R693K} (LV-Cub-6K2 plus NubG-Sec24a^{R693K}); III, 6K₂ plus Sec24a (LV-Cub-6K2 plus NubG-Sec24a). (B) WT and *g92 A. thaliana* plants were inoculated with TuMV/6K₂:GFP and observed under UV light 11 days later. White arrows indicate the viral inoculation site. (C) The upper nonagroinfiltrated leaves of the WT and *g92 A. thaliana* plants infected with TuMV/6K₂:GFP were collected at 11 dpi and analyzed for virus production by immunoblot analysis using a rabbit anti-CP serum. (D) Protoplasts were isolated from WT and *g92 A. thaliana* plants and were mock transfected or transfected with p35STuMV^{VNN} and p35STuMV. Production of CP was analyzed 40 h after transfection using an anti-TuMV CP rabbit serum. Confocal images of TuMV/6K₂:mCherry//GFP-HDEL-infiltrated WT (E) and *g92* (F) *A. thaliana* epidermal cells are shown at 8 and 12 dpi. These images are three-dimensional renderings of 60 1- μ m-thick slices that overlap by 0.5 μ m. Scale bar, 20 μ m.

case of the Norwalk virus, the nonstructural protein p22, which inhibits COPII vesicle trafficking, contains the YX Φ ESDG motif (61). The DSSP domain in the N- and the lysine residue in the C-terminal tail of MNSV p7B are required for ER export (62). On the other hand, no clearly defined ER export motifs were identified for the TGBp3 of BaMV (17).

These N-terminal 18 residues were predicted to be exposed in the cytosol (Fig. 1) and were found to possibly interact with membrane-associated host factors (i.e., proteins or lipids) (Fig. 2). One host factor turned out to be Sec24a (Fig. 8), which is consistent with the current model where Sec24a binds the cytoplasmic tail of the cargo membrane proteins for their ER export (20). Sec24 is the

TABLE 2 Systemic viral infection of WT versus *g92* mutant *A. thaliana*

<i>A. thaliana</i> wild type or mutant	No. of plants systemically infected/ total infected	
	11 dpi	13 dpi
Expt 1		
WT	12/16	14/16
<i>g92</i> mutant	0/16	7/16
Expt 2		
WT	14/16	14/16
<i>g92</i> mutant	2/16	8/16
Expt 3		
WT	11/16	13/16
<i>g92</i> mutant	1/16	6/16

main COPII coat protein that recognizes specific sorting sequences in cargo proteins and has multiple independent cargo-binding sites, which provides the required plasticity for selecting cargo molecules with distinct sorting signals (63). Sec24a binding to cargo membrane proteins is dynamic as this complex disassembles as soon as the vesicle buds off from the ER. Once this takes place, Sec24a is recycled back to the ERES (20). This dynamic interaction explains the partial colocalization of Sec24a with 6K₂-induced vesicles (Fig. 7). It is only when ER-to-Golgi apparatus trafficking is stalled by the addition of BFA that near complete colocalization can be observed. Hanton et al. (64) showed that treatment with 100 μg/ml BFA caused the redistribution of ERES markers to the cytosol. A lower BFA concentration (10 μg/ml) in our case may explain the discrepancy between the two outcomes.

The biological significance of the interaction between Sec24a and 6K₂ was supported by the delayed systemic infection of the *A. thaliana g92* mutant line (Fig. 9). Because Sec24a is essential for plant viability, it cannot be excluded that the partial loss of function of this protein may have pleomorphic rather than have specific effects on virus infection. We think, however, that the defective Sec24a would have a direct impact on virus infection. The partial loss of function of Sec24a in *g92* plants caused unique ER morphology defects and inhibition of protein secretion (57, 65). The same membrane rearrangement and inhibition of protein secretion were observed in TuMV-infected cells (25). Possibly, the same effect points to the same cause—Sec24a function has been modified. The difference is that the R693K mutation alters Sec24a activity in *g92* plants, while 6K₂ coopts Sec24a function and thus affects its ability to function normally in ER-to-Golgi apparatus vesicular trafficking in TuMV-infected cells.

Replacement of the tryptophan residue of 6K₂ with an alanine within the polyprotein (i.e., TuMV^{W15A}) affected TuMV infection. The end result was a reduced level of cellular virus production, with no indication of plant systemic viral infection (Fig. 5). The reduced virus production at the cellular level could be the reason why no virus movement was observed. However, we would have expected a delayed systemic infection since TuMV^{W15A} cellular production was still significant, being half the level of what was obtained for WT TuMV. There was, however, no systemic infection, even after 2 weeks, when normally it is observed at 5 dpi with WT TuMV. Furthermore, the way we analyze cell-to-cell movement is very sensitive, and we can easily distinguish movement at a single-cell layer, but we did not observe any cell-to-cell

movement for TuMV^{W15A}/6K₂:mCherry (Fig. 6). Consequently, it does not appear that reduced virus production is the reason for the lack of virus movement. The recent observation that plant virus replication and movement are coupled events (14) suggests that they should be considered a unit, where replication and movement cannot be separated from each other. This also appears to be the case for TuMV (27). Thus, we think that the W15A mutation has a primary effect on virus movement, with an overflow effect on virus production.

6K₂ is found in the form of 6K₂-VPg-Pro in infected cells (28), and VPg has been proposed to act as a hub protein for the assembly of the replication complex (66). This suggests that a much larger protein complex exists as a result of 6K₂ being recognized as a cargo membrane protein. We thus propose that by interacting with Sec24a, 6K₂ is able to engage the host cell ER export machinery to initiate viral vesicular formation for transport of vRNA and viral as well as host proteins that are necessary for virus systemic movement.

ACKNOWLEDGMENTS

This work was supported by grants from the Natural Science and Engineering Research Council (NSERC) of Canada and from Le Fonds Québécois de Recherche sur la Nature et les Technologies (FQRNT) to H.Z. and J.F.L.

We thank Jessy Tremblay for helping with confocal microscopy and Federica Brandizzi for *A. thaliana g92* seeds. We thank Peter Moffett for critically reading the manuscript.

REFERENCES

- den Boon JA, Ahlquist P. 2010. Organelle-like membrane compartmentalization of positive-strand RNA virus replication factories. *Annu Rev Microbiol* 64:241–256. <http://dx.doi.org/10.1146/annurev.micro.112408.134012>.
- Laliberté J-F, Sanfaçon H. 2010. Cellular remodeling during plant virus infection. *Annu Rev Phytopathol* 48:69–91. <http://dx.doi.org/10.1146/annurev-phyto-073009-114239>.
- Belov GA, Nair V, Hansen BT, Hoyt FH, Fischer ER, Ehrenfeld E. 2012. Complex dynamic development of poliovirus membranous replication complexes. *J Virol* 86:302–312. <http://dx.doi.org/10.1128/JVI.05937-11>.
- Knoops K, Kikkert M, Worm SH, Zevenhoven-Dobbe JC, van der Meer Y, Koster AJ, Mommaas AM, Snijder EJ. 2008. SARS-coronavirus replication is supported by a reticulovesicular network of modified endoplasmic reticulum. *PLoS Biol* 6:e226. <http://dx.doi.org/10.1371/journal.pbio.0060226>.
- Knoops K, Bárcena M, Limpens RWAL, Koster AJ, Mommaas AM, Snijder EJ. 2012. Ultrastructural characterization of arterivirus replication structures: reshaping the endoplasmic reticulum to accommodate viral RNA synthesis. *J Virol* 86:2474–2487. <http://dx.doi.org/10.1128/JVI.06677-11>.
- Carette JE, Stuijver M, Van Lent J, Wellink J, Van Kammen A. 2000. Cowpea mosaic virus infection induces a massive proliferation of endoplasmic reticulum but not Golgi membranes and is dependent on de novo membrane synthesis. *J Virol* 74:6556–6563. <http://dx.doi.org/10.1128/JVI.74.14.6556-6563.2000>.
- Hwang Y, McCartney A, Gidda S, Mullen R. 2008. Localization of the carnation Italian ringspot virus replication protein p36 to the mitochondrial outer membrane is mediated by an internal targeting signal and the TOM complex. *BMC Cell Biol* 9:54. <http://dx.doi.org/10.1186/1471-2121-9-54>.
- Prod'homme D, Jakubiec A, Tournier V, Drugeon G, Jupin I. 2003. Targeting of the turnip yellow mosaic virus 66K replication protein to the chloroplast envelope is mediated by the 140K protein. *J Virol* 77:9124–9135. <http://dx.doi.org/10.1128/JVI.77.17.9124-9135.2003>.
- McCartney AW, Greenwood JS, Fabian MR, White KA, Mullen RT. 2005. Localization of the tomato bushy stunt virus replication protein p33 reveals a peroxisome-to-endoplasmic reticulum sorting pathway. *Plant Cell* 17:3513–3531. <http://dx.doi.org/10.1105/tpc.105.036350>.

10. Nagy PD, Pogany J. 2012. The dependence of viral RNA replication on co-opted host factors. *Nat Rev Microbiol* 10:137–149. <http://dx.doi.org/10.1038/nrmicro2692>.
11. Diaz A, Ahlquist P. 2012. Role of host reticulon proteins in rearranging membranes for positive-strand RNA virus replication. *Curr Opin Microbiol* 15:519–524. <http://dx.doi.org/10.1016/j.mib.2012.04.007>.
12. Verchot J. 2012. Cellular chaperones and folding enzymes are vital contributors to membrane bound replication and movement complexes during plant RNA virus infection. *Front Plant Sci* 3:275. <http://dx.doi.org/10.3389/fpls.2012.00275>.
13. Schwartz M, Chen J, Janda M, Sullivan M, den Boon J, Ahlquist P. 2002. A positive-strand RNA virus replication complex parallels form and function of retrovirus capsids. *Mol Cell* 9:505–514. [http://dx.doi.org/10.1016/S1097-2765\(02\)00474-4](http://dx.doi.org/10.1016/S1097-2765(02)00474-4).
14. Tilsner J, Linnik O, Louveaux M, Roberts IM, Chapman SN, Oparka KJ. 2013. Replication and trafficking of a plant virus are coupled at the entrances of plasmodesmata. *J Cell Biol* 201:981–995. <http://dx.doi.org/10.1083/jcb.201304003>.
15. Kusumanegara K, Mine A, Hyodo K, Kaido M, Mise K, Okuno T. 2012. Identification of domains in p27 auxiliary replicase protein essential for its association with the endoplasmic reticulum membranes in Red clover necrotic mosaic virus. *Virology* 433:131–141. <http://dx.doi.org/10.1016/j.virol.2012.07.017>.
16. Genovés A, Pallás V, Navarro JA. 2011. Contribution of topology determinants of a viral movement protein to its membrane association, intracellular traffic, and viral cell-to-cell movement. *J Virol* 85:7797–7809. <http://dx.doi.org/10.1128/JVI.02465-10>.
17. Wu C-H, Lee S-C, Wang C-W. 2011. Viral protein targeting to the cortical endoplasmic reticulum is required for cell-cell spreading in plants. *J Cell Biol* 193:521–535. <http://dx.doi.org/10.1083/jcb.201006023>.
18. Wei T, Zhang C, Hou X, Sanfacon H, Wang A. 2013. The SNARE protein Syp71 is essential for turnip mosaic virus infection by mediating fusion of virus-induced vesicles with chloroplasts. *PLoS Pathog* 9:e1003378. <http://dx.doi.org/10.1371/journal.ppat.1003378>.
19. Hyodo K, Mine A, Taniguchi T, Kaido M, Mise K, Taniguchi H, Okuno T. 2013. ADP ribosylation factor 1 plays an essential role in the replication of a plant RNA virus. *J Virol* 87:163–176. <http://dx.doi.org/10.1128/JVI.02383-12>.
20. Brandizzi F, Barlowe C. 2013. Organization of the ER-Golgi interface for membrane traffic control. *Nat Rev Mol Cell Biol* 14:382–392. <http://dx.doi.org/10.1038/nrm3588>.
21. Barajas D, Jiang Y, Nagy PD. 2009. A unique role for the host ESCRT proteins in replication of tomato bushy stunt virus. *PLoS Pathog* 5:e1000705. <http://dx.doi.org/10.1371/journal.ppat.1000705>.
22. Barajas D, Nagy PD. 2010. Ubiquitination of tombusvirus p33 replication protein plays a role in virus replication and binding to the host Vps23p ESCRT protein. *Virology* 397:358–368. <http://dx.doi.org/10.1016/j.virol.2009.11.010>.
23. Diaz A, Wang X, Ahlquist P. 2010. Membrane-shaping host reticulon proteins play crucial roles in viral RNA replication compartment formation and function. *Proc Natl Acad Sci U S A* 107:16291–16296. <http://dx.doi.org/10.1073/pnas.1011105107>.
24. Mayo MA. 1995. The Potyviridae. *New Phytologist* 131:289–290. <http://dx.doi.org/10.1111/j.1469-8137.1995.tb05732.x>.
25. Grangeon R, Agbeci M, Chen J, Grondin G, Zheng H, Laliberté J-F. 2012. Impact on the endoplasmic reticulum and Golgi apparatus of turnip mosaic virus infection. *J Virol* 86:9255–9265. <http://dx.doi.org/10.1128/JVI.01146-12>.
26. Cotton S, Grangeon R, Thivierge K, Mathieu I, Ide C, Wei T, Wang A, Laliberté J-F. 2009. Turnip mosaic virus RNA replication complex vesicles are mobile, align with microfilaments, and are each derived from a single viral genome. *J Virol* 83:10460–10471. <http://dx.doi.org/10.1128/JVI.00819-09>.
27. Grangeon R, Jiang J, Wan J, Agbeci M, Zheng H, Laliberté J-F. 2013. 6K2-induced vesicles can move cell to cell during turnip mosaic virus infection. *Front Microbiol* 4:351. <http://dx.doi.org/10.3389/fmicb.2013.00351>.
28. Beauchemin C, Boutet N, Laliberté J-F. 2007. Visualization of the interaction between the precursors of VPg, the viral protein linked to the genome of turnip mosaic virus, and the translation eukaryotic initiation factor iso 4E in planta. *J Virol* 81:775–782. <http://dx.doi.org/10.1128/JVI.01277-06>.
29. Wei T, Wang A. 2008. Biogenesis of cytoplasmic membranous vesicles for plant potyvirus replication occurs at endoplasmic reticulum exit sites in a COPI- and COPII-dependent manner. *J Virol* 82:12252–12264. <http://dx.doi.org/10.1128/JVI.01329-08>.
30. Krogh A, Larsson B, von Heijne G, Sonnhammer EL. 2001. Predicting transmembrane protein topology with a hidden Markov model: application to complete genomes. *J Mol Biol* 305:567–580. <http://dx.doi.org/10.1006/jmbi.2000.4315>.
31. Hirokawa T, Boon-Chieng S, Mitaku S. 1998. SOSUI: classification and secondary structure prediction system for membrane proteins. *Bioinformatics* 14:378–379. <http://dx.doi.org/10.1093/bioinformatics/14.4.378>.
32. Claros MG, von Heijne G. 1994. TopPred II: an improved software for membrane protein structure predictions. *Comput Appl Biosci* 10:685–686.
33. Hessa T, Kim H, Bihlmaier K, Lundin C, Boekel J, Andersson H, Nilsson I, White SH, von Heijne G. 2005. Recognition of transmembrane helices by the endoplasmic reticulum translocon. *Nature* 433:377–381. <http://dx.doi.org/10.1038/nature03216>.
34. Jones DT, Taylor WR, Thornton JM. 1994. A model recognition approach to the prediction of all-helical membrane protein structure and topology. *Biochemistry* 33:3038–3049. <http://dx.doi.org/10.1021/bi00176a037>.
35. Cserzo M, Wallin E, Simon I, von Heijne G, Elofsson A. 1997. Prediction of transmembrane alpha-helices in prokaryotic membrane proteins: the dense alignment surface method. *Protein Eng* 10:673–676. <http://dx.doi.org/10.1093/protein/10.6.673>.
36. Rost B, Yachdav G, Liu J. 2004. The PredictProtein server. *Nucleic Acids Res* 32:W321–W326. <http://dx.doi.org/10.1093/nar/gkh377>.
37. Juretic D, Zoranic L, Zucic D. 2002. Basic charge clusters and predictions of membrane protein topology. *J Chem Infect Comput Sci* 42:620–632. <http://dx.doi.org/10.1021/ci010263s>.
38. Jayasinghe S, Hristova K, White SH. 2001. MPTopo: a database of membrane protein topology. *Protein Sci* 10:455–458. <http://dx.doi.org/10.1110/ps.43501>.
39. Thivierge K, Cotton S, Dufresne PJ, Mathieu I, Beauchemin C, Ide C, Fortin MG, Laliberté J-F. 2008. Eukaryotic elongation factor 1A interacts with turnip mosaic virus RNA-dependent RNA polymerase and VPg-Pro in virus-induced vesicles. *Virology* 377:216–225. <http://dx.doi.org/10.1016/j.virol.2008.04.015>.
40. Beauchemin C, Bougie V, Laliberté J-F. 2005. Simultaneous production of two foreign proteins from a potyvirus-based vector. *Virus Res* 112:1–8. <http://dx.doi.org/10.1016/j.virusres.2005.03.001>.
41. Sparkes IA, Runions J, Kearns A, Hawes C. 2006. Rapid, transient expression of fluorescent fusion proteins in tobacco plants and generation of stably transformed plants. *Nat Protoc* 1:2019–2025. <http://dx.doi.org/10.1038/nprot.2006.286>.
42. Chen J, Stefano G, Brandizzi F, Zheng H. 2011. *Arabidopsis* RHD3 mediates the generation of the tubular ER network and is required for Golgi distribution and motility in plant cells. *J Cell Sci* 124:2241–2252. <http://dx.doi.org/10.1242/jcs.084624>.
43. Yoo SD, Cho YH, Sheen J. 2007. *Arabidopsis* mesophyll protoplasts: a versatile cell system for transient gene expression analysis. *Nat Protoc* 2:1565–1572. <http://dx.doi.org/10.1038/nprot.2007.199>.
44. Grefen C, Lalonde S, Obrdlík P. 2001. Split-ubiquitin system for identifying protein-protein interactions in membrane and full-length proteins. *Curr Protoc Neurosci* 41:5.27.5.27.1–5.27.41. <http://dx.doi.org/10.1002/0471142301.ns0527s41>.
45. Beauchemin C, Laliberté J-F. 2007. The poly(A) binding protein is internalized in virus-induced vesicles or redistributed to the nucleolus during turnip mosaic virus infection. *J Virol* 81:10905–10913. <http://dx.doi.org/10.1128/JVI.01243-07>.
46. von Heijne G. 1992. Membrane protein structure prediction: hydrophobicity analysis and the positive-inside rule. *J Mol Biol* 225:487–494. [http://dx.doi.org/10.1016/0022-2836\(92\)90934-C](http://dx.doi.org/10.1016/0022-2836(92)90934-C).
47. von Heijne G, Gavel Y. 1988. Topogenic signals in integral membrane proteins. *Eur J Biochem* 174:671–678. <http://dx.doi.org/10.1111/j.1432-1033.1988.tb14150.x>.
48. Brandizzi F, Snapp EL, Roberts AG, Lippincott-Schwartz J, Hawes C. 2002. Membrane protein transport between the endoplasmic reticulum and the Golgi in tobacco leaves is energy dependent but cytoskeleton independent: evidence from selective photobleaching. *Plant Cell* 14:1293–1309. <http://dx.doi.org/10.1105/tpc.001586>.
49. Barlowe C. 2003. Signals for COPII-dependent export from the ER: what's the ticket out? *Trends Cell Biol* 13:295–300. [http://dx.doi.org/10.1016/S0962-8924\(03\)00082-5](http://dx.doi.org/10.1016/S0962-8924(03)00082-5).
50. Dunn KW, Kamocka MM, McDonald JH. 2011. A practical guide to

- evaluating colocalization in biological microscopy. *Am J Physiol Cell Physiol* 300:C723–C742. <http://dx.doi.org/10.1152/ajpcell.00462.2010>.
51. Giraudo CG, Maccioni HJF. 2003. Endoplasmic reticulum export of glycosyltransferases depends on interaction of a cytoplasmic dibasic motif with Sar1. *Mol Biol Cell* 14:3753–3766. <http://dx.doi.org/10.1091/mbc.E03-02-0101>.
 52. Schoberer J, Vavra U, Stadlmann J, Hawes C, Mach L, Steinkellner H, Strasser R. 2009. Arginine/lysine residues in the cytoplasmic tail promote ER export of plant glycosylation enzymes. *Traffic* 10:101–115. <http://dx.doi.org/10.1111/j.1600-0854.2008.00841.x>.
 53. Li XH, Carrington JC. 1995. Complementation of tobacco etch potyvirus mutants by active RNA polymerase expressed in transgenic cells. *Proc Natl Acad Sci U S A* 92:457–461. <http://dx.doi.org/10.1073/pnas.92.2.457>.
 54. Agbeci M, Grangeon R, Nelson RS, Zheng H, Laliberté J-F. 2013. Contribution of host intracellular transport machineries to intercellular movement of turnip mosaic virus. *PLoS Pathog* 9:e1003683. <http://dx.doi.org/10.1371/journal.ppat.1003683>.
 55. Tanaka Y, Nishimura K, Kawamukai M, Oshima A, Nakagawa T. 2013. Redundant function of two *Arabidopsis* COPII components, AtSec24B and AtSec24C, is essential for male and female gametogenesis. *Planta* 238: 561–575. <http://dx.doi.org/10.1007/s00425-013-1913-1>.
 56. Nebenfuhr A, Ritzenthaler C, Robinson DG. 2002. Brefeldin A: deciphering an enigmatic inhibitor of secretion. *Plant Physiol* 130:1102–1108. <http://dx.doi.org/10.1104/pp.011569>.
 57. Faso C, Chen YN, Tamura K, Held M, Zemelis S, Marti L, Saravanan R, Hummel E, Kung L, Miller E, Hawes C, Brandizzi F. 2009. A missense mutation in the *Arabidopsis* COPII coat protein Sec24A induces the formation of clusters of the endoplasmic reticulum and Golgi apparatus. *Plant Cell* 21:3655–3671. <http://dx.doi.org/10.1105/tpc.109.068262>.
 58. Lerich A, Langhans M, Sturm S, Robinson DG. 2011. Is the 6 kDa tobacco etch viral protein a bona fide ERES marker? *J Exp Bot* 62:5013–5023. <http://dx.doi.org/10.1093/jxb/err200>.
 59. Peiró A, Martínez-Gil L, Tamborero S, Pallás V, Sánchez-Navarro JA, Mingarro I. 2014. The tobacco mosaic virus movement protein associates with but does not integrate into biological membranes. *J Virol* 88:3016–3026. <http://dx.doi.org/10.1128/JVI.03648-13>.
 60. Franke M, Bräulke T, Storch S. 2013. Transport of the GlcNAc-1-phosphotransferase α/β -subunit precursor protein to the Golgi apparatus requires a combinatorial sorting motif. *J Biol Chem* 288:1238–1249. <http://dx.doi.org/10.1074/jbc.M112.407676>.
 61. Sharp TM, Guix S, Katayama K, Crawford SE, Estes MK. 2010. Inhibition of cellular protein secretion by Norwalk virus nonstructural protein p22 requires a mimic of an endoplasmic reticulum export signal. *PLoS One* 5:e13130. <http://dx.doi.org/10.1371/journal.pone.0013130>.
 62. Serra-Soriano M, Pallás V, Navarro JA. 2014. A model for transport of a viral membrane protein through the early secretory pathway: minimal sequence and endoplasmic reticulum lateral mobility requirements. *Plant J* 77:863–879. <http://dx.doi.org/10.1111/tpj.12435>.
 63. Miller EA, Beilharz TH, Malkus PN, Lee MCS, Hamamoto S, Orci L, Schekman R. 2003. Multiple cargo binding sites on the COPII subunit Sec24p ensure capture of diverse membrane proteins into transport vesicles. *Cell* 114:497–509. [http://dx.doi.org/10.1016/S0092-8674\(03\)00609-3](http://dx.doi.org/10.1016/S0092-8674(03)00609-3).
 64. Hanton SL, Matheson LA, Chatre L, Brandizzi F. 2009. Dynamic organization of COPII coat proteins at endoplasmic reticulum export sites in plant cells. *Plant J* 57:963–974. <http://dx.doi.org/10.1111/j.1365-3113X.2008.03740.x>.
 65. Nakano RT, Matsushima R, Ueda H, Tamura K, Shimada T, Li L, Hayashi Y, Kondo M, Nishimura M, Hara-Nishimura I. 2009. GNOM-LIKE1/ERMO1 and SEC24a/ERMO2 are required for maintenance of endoplasmic reticulum morphology in *Arabidopsis thaliana*. *Plant Cell* 21: 3672–3685. <http://dx.doi.org/10.1105/tpc.109.068270>.
 66. Jiang J, Laliberté JF. 2011. The genome-linked protein VPg of plant viruses—a protein with many partners. *Curr Opin Virol* 1:347–354. <http://dx.doi.org/10.1016/j.coviro.2011.09.010>.